BURKHARD RITTER

FORMATION OF LOCAL MOMENTS AND THE KONDO EFFECT IN THE SINGLE IMPURITY ANDERSON MODEL: A DIAGRAMMATIC DETERMINANTAL CONTINUOUS-TIME QUANTUM MONTE CARLO STUDY

FORMATION OF LOCAL MOMENTS AND THE KONDO EFFECT IN THE SINGLE IMPURITY ANDERSON MODEL: A DIAGRAMMATIC DETERMINANTAL CONTINUOUS-TIME QUANTUM MONTE CARLO STUDY

BURKHARD RITTER

Supervised by Prof. Dr. Fakher F. Assaad

Institut für Theoretische Physik und Astrophysik
Julius-Maximilians-Universität Würzburg

December 2009

ABSTRACT

We apply the weak-coupling diagrammatic determinantal continuous-time quantum Monte Carlo method to the single impurity Anderson model. A modern and efficient C++ program is devised, implemented and, consecutively, thoroughly tested. The accuracy and reliability of the program is verified. The code is used for the study of the formation of local moments and of the Kondo effect. To this end, thermodynamic as well as dynamic properties – the latter extracted with the Maximum Entropy method – are measured over temperature and for different impurity energy levels. A local moment is seen to arise at intermediate temperatures. At a very low temperature the Kondo effect emerges. Varying the impurity levels over the bandwidth of the host metal, the local moment regime is identified, its breakdown observed and discussed.

ZUSAMMENFASSUNG

Wir benutzen die diagrammatische, in der Zeit kontinuierliche Quanten-Monte-Carlo-Methode für die Untersuchung des einfachen Anderson-Störstellenmodells. Dazu wurde ein modernes und effizientes C++-Programm entworfen, implementiert und anschließend auf Mark und Knochen getestet. Die Genauigkeit und Zuverlässigkeit des Programms ward verifiziert. Es fand dann Anwendung bei der Untersuchung der Ausbildung von lokalen magnetischen Momenten, sowie des Kondo-Effekts. Thermodynamische wie auch dynamische Größen – letztere gewonnen durch die Methode der maximalen Entropie – wurden über die Temperatur und für verschiedene Störstellenniveaus gemessen. Bei nicht zu hohen Temperaturen bildet sich ein lokales Moment aus. Bei sehr tiefen Temperaturen kann der Kondo-Effekt beobachtet werden. Die Niveaus der Störstelle über die ganze Bandbreite des Gastsystems variierend, sind wir in der Lage, das Regime des lokalen Moments zu identifizieren, und auch das Zerfallen desselben zu beobachten.

CONTENTS

LIST OF FIGURES

ACRONYMS

SIAM   Single Impurity Anderson Model

PAM   Periodic Anderson Model

DDQMC   Diagrammatic Determinantal Quantum Monte Carlo

CTQMC   Continuous-Time Quantum Monte Carlo

DMFT   Dynamical Mean-Field Theory

MaxEnt   Maximum Entropy

PES   Photoemission Spectroscopy

IPES   Inverse Photoemission Spectroscopy

INTRODUCTION

The formation of local moments was first studied by P. W. Anderson in 1961 [1]. It was around the same time that experimentalists had related anomalies observed at low temperatures in various metals to a dilute concentration of impurities in those systems. The impurities were seen to carry a local magnetic moment, contributing a Curie-Weiss term to the magnetic susceptibility. One striking aspect of the anomalous behaviour was a minimum in resistivity. In contrast, the conventional Mathiessen's rule suggests a monotone decline of the resistivity as the temperature is lowered. Naturally, the desire to understand these exciting phenomena sparked interest in the nature and formation of the local moment of the impurities. Before Anderson, impurities in a metallic host were mainly treated as scattering potentials. Friedel had shown in the fifties that such a potential within the conduction band of the host system would lead to highly localised states – "virtual bound" states. Anderson approached the problem from a different direction. He modelled the impurity as a near-atomic state that would hybridise with the states of the host system. By including an on-site Coulomb-interaction term for the impurity he was able to derive a criterion for the local moment formation employing a Hartree-Fock approximation. His model was to become known as the single impurity Anderson model, short SIAM.

The s-d model takes another approach to the solute impurity problem. In contrast to the Anderson model it explicitly presumes the presence of a local moment and models the interaction between the impurity and host metal as a spin-spin Heisenberg exchange interaction. Treating this model to third order perturbation theory, in 1964 Kondo was able to explain the resistance minimum that had hitherto puzzled the community. This was a great success. Another outcome of an extended perturbative treatment of the s-d model was the Curie-Weiss behaviour for the susceptibility observed in experiment. However, Kondo's explanation had a very pronounced draw-back: As a result of the perturbative nature of his method, the resistivity, susceptibility and other quantities diverged at low temperatures. Kondo's original results diverged at a temperature of zero, but a refined calculation showed that the divergence already happens at a finite tempertature – the Kondo temperature. The challenge to find a satisfactory theory for the low temperature behaviour became the Kondo problem. It

was again Anderson who worked out a first clue at a possible solution by the end of the sixties. He introduced the idea of scaling to the Kondo problem. His "Poor man's scaling approach" [2] successively integrates out high-energy excitations to obtain an effective low-energy model. Although his treatment, being perturbative, could not be carried out to very low temperatures, Anderson forecast that the coupling between impurity and bath would increase indefinitely. As it had been established earlier that the coupling was antiferromagnetic in nature, this would consequently lead to an entangled spin-singlet state which effectively screens the spin of the impurity.

K. G. Wilson built on Anderson's scaling ideas. He applied his newly developed numerical Renormalization Group method to the Kondo problem in the early seventies and was not only able to confirm Anderson's qualitative assertions, but was also the first to obtain definite quantitative results for the low temperature regime. Although some exciting developments were to follow later on, for example the exact solutions via the Bethe ansatz, with Wilson's results an understanding of the Kondo problem was basically established. For one of the first times did the heavy reliance on numerical and computational resources provide the key to the understanding of a physical problem.

Another numerical, but quite different approach to the impurity problem was proposed by J. E. Hirsch and R. M. Fye in 1986 [3]. It is a fermionic Quantum Monte Carlo algorithm and became known – not altogether surprising – as the Hirsch-Fye method. To this day it is one of the most popular methods for the numerical treatment of impurities. The Hirsch-Fye approach discretises the imaginary time and evokes a Trotter decomposition to cast the partition function into a suitable form, introducing a systematic error. It then employs a discrete Hubbard-Stratonovich transformation [4] to decouple the interaction term. Finally, the configuration space of the auxiliary fields is sampled with a Monte Carlo procedure. Apart from the systematic error, the time discretisation may become a problem at low temperature by itself. In this regime, the Green's function, one of the primary quantities of interest, often varies strongly over imaginary time. To resolve the delicate features of the function a finer discretisation is required. However, a better time discretisation becomes very costly computationally.

In 2005 A. N. Rubtsov et al. proposed a new method, the diagrammatic determinantal Quantum Monte Carlo method, short DDQMC [5]. Alternatively, the method is sometimes simply referred to as CTQMC (continuous-time QMC), accounting for the important fact that the method is continuous in the imaginary time. Thus it avoids the systematic error of the Hirsch-Fye approach and is exact within the numerical

precision limits. Moreover, it does not resort to the Hubbard-Stratonovich transformation and therefore, in principle, does not rely on auxiliary fields. Practically, in most common cases a static or dynamic Ising field is introduced to keep the sign problem at bay. The DDQMC method is simple. Following common perturbation theory, the partition function is expanded in orders of the interaction parameter and Wick's theorem is applied. Each order can be represented diagrammatically. The DDQMC method directly takes all vertices of a given order and casts them into a determinantal form. The determinant is identified as the weight of the configuration. The partition function may then be sampled stochastically, summing up all diagrams of the expansion. The DDQMC method is very flexible. It is applicable to a wide array of problems, the one and two dimensional Hubbard models as well as the Anderson model being popular examples. Originally developed in the weak-coupling limit, it can readily be reformulated for the strong-coupling case. For an impurity problem this means the expansion in the hybridisation instead of the interaction parameter [6]. The method has been extended to real times, using a Keldysh formalism, allowing for the study of non-equilibrium physics [7].

Methods to tackle impurity problems have seen an upsurge with the development of the dynamical mean-field theory (DMFT) in the 90s [8]. This approach maps a lattice model to an impurity problem and is exact in the limit of infinite dimensionality. The impurity model is solved with an effective bath hybridisation, which has to be calculated self-consistently. In recent years the DMFT method has been used extensively for the study of strongly correlated electron systems. One of the most popular choices for a numerical impurity solver for DMFT is the Hirsch-Fye algorithm. However, with the availability of the DDQMC method, this new approach has become a viable and often even preferable choice as an impurity solver as well (see, for an example, [9]).

In this thesis we set out to implement the DDQMC method from scratch. We cast the algorithm into a modern, efficient and well-tested C++ code. The Anderson model is implemented to investigate a single impurity in a host metal. We are particularly interested in the formation of the local moment. To this end the double occupancy, the spin susceptibility and the Green's function are measured over a wide temperature range. Furthermore, the impurity levels are shifted from the lower to the upper band edge of the host metal, at a fixed temperature. From the calculated Green's function the spectral function is extracted by means of the Maximum Entropy method. Spectral functions provide a most intuitive picture of the physical processes. At low temperatures we observe the Kondo effect. As already the formation of the local

moment, the development of the Kondo effect and its signature imprints on the calculated observables are of particular interest.

In the first chapter the weak-coupling DDQMC algorithm is laid out in a very generic way. The physical ideas, the Monte Carlo procedure and some simple mathematical tricks to speed up the algorithm are discussed in detail. A few words about the practical implementation of the method conclude the chapter. The Anderson model is presented in the succeeding chapter. After physically motivating the complete Hamiltonian, the local hybridisation approximation simplifies the model. Then the application of the DDQMC method to the Anderson model is discussed at length. A short excursion to the model and selected observables under a particle-hole transformation follows, before the s-d model is briefly stated and related to the Anderson model. The final chapter presents the results obtained by the simulations. The careful examination and evaluation of the measurements of the double occupancy, the spin susceptibility and the spectral function lead up to the discussion of the emergent physical picture.

THE DIAGRAMMATIC DETERMINANTAL QUANTUM MONTE CARLO METHOD

We derive the diagrammatic determinantal quantum Monte Carlo method (DDQMC) for a general two-particle interaction problem. To this end we first briefly revise the time-ordered exponential as presented in standard many-body text books [10], [11]. Subsequently, the exponential is expanded and cast into a determinantal form, employing Wick's theorem. Monte Carlo methods are discussed as a device to stochastically evaluate the time-ordered exponential and compute the expectation value of observables. A concrete sampling scheme is presented and after a short discussion of the scalability, a very efficient update mechanism is derived. We conclude the chapter with a few words about the practical implementation of the algorithm. We follow [12] in terminology and presentation.

2.1 THE TIME-ORDERED EXPONENTIAL

We consider a Hamiltonian

$$H = H_0 + V = \sum_{\alpha\beta} t_{\alpha\beta} c_\alpha^\dagger c_\beta + \sum_{\alpha\beta\gamma\delta} U_{\alpha\beta\delta\gamma} c_\alpha^\dagger c_\beta c_\gamma^\dagger c_\delta \tag{2.1}$$

with a non-interacting part H_0 and a two-particle interaction part V. $c_\alpha^\dagger$ creates a fermion in orbital α, c_β annihilates a fermion in orbital β. Our long term goal is to compute thermal expectation values of observables $O(\tau)$.

$$\langle O(\tau) \rangle = \text{Tr}\,\rho O(\tau) = \text{Tr}\,\frac{e^{-\beta H}}{Z} O(\tau) \tag{2.2}$$

Here ρ is the density matrix, $Z = \text{Tr}\,e^{-\beta H}$ the partition function and β the inverse temperature. The imaginary time is represented by τ and $-\beta \leqslant \tau \leqslant \beta$. The time dependent observable $O(\tau) = e^{\tau H} O e^{-\tau H}$ is understood in the modified Heisenberg

picture. However, for the task at hand the interaction picture is more convenient. So let us rewrite the expectation value

$$
\begin{aligned}
\langle O(\tau) \rangle &= \text{Tr} \, \frac{e^{-\beta H}}{Z} \, e^{\tau H} O e^{-\tau H} \\
&= \frac{Z_0}{Z} \, \text{Tr} \, \frac{e^{-\beta H_0}}{Z_0} e^{\beta H_0} e^{-\beta H} \, e^{\tau H} O e^{-\tau H} \\
&= \frac{Z_0}{Z} \, \langle e^{\beta H_0} e^{-\beta H} \, e^{\tau H} \, e^{-\tau H_0} e^{\tau H_0} \, O \, e^{-\tau H_0} e^{\tau H_0} \, e^{-\tau H} \rangle_0 \\
&= \frac{Z_0}{Z} \, \langle S(\beta,0) S(0,\tau) O(\tau) S(\tau,0) \rangle_0
\end{aligned}
\tag{2.3}
$$

where we have cast the observable to the interaction representation, $O(\tau) = e^{\tau H_0} O e^{-\tau H_0}$, and $\langle \bullet \rangle_0$ denotes the expectation value with respect to the unperturbed system H_0. The time-evolution operator takes the form

$$
S(\tau_f, \tau_i) = e^{\tau_f H_0} e^{-(\tau_f - \tau_i) H} e^{-\tau_i H_0}
\tag{2.4}
$$

evolving a state from the initial time τ_i to the final time τ_f. From the fundamental property of the density matrix $\text{Tr} \, \rho = 1$ and (2.3) we immediately get an expression for the partition function

$$
\frac{Z}{Z_0} = \langle S(\beta,0) \rangle_0 \; .
\tag{2.5}
$$

Thus we write for the observable

$$
\langle O(\tau) \rangle = \frac{\langle S(\beta,\tau) O(\tau) S(\tau,0) \rangle_0}{\langle S(\beta,0) \rangle_0} \; .
\tag{2.6}
$$

So far the expectation value is hardly any easier to evaluate than in the beginning. However, we've reformulated the problem so that the task is now to find a computable expression for the time-evolution operator S.

To this end we notice that, being a time-evolution operator, S fulfils the composition property. Consequently, we can decompose every time span into an infinite number of time slices, conceptually reminiscent of Feynman path integrals.

$$
\begin{aligned}
S(\tau_f, \tau_i) &= S(\tau_f, \tau_l) S(\tau_l, \tau_i) \\
&= S(\tau_f, \tau_{n-1}) S(\tau_{n-1}, \tau_{n-2}) \ldots S(\tau_2, \tau_1) S(\tau_1, \tau_i)
\end{aligned}
\tag{2.7}
$$

For each infinitesimal time $\Delta\tau = \frac{\tau_f - \tau_i}{n}$ with $n \to \infty$ we apply a Trotter decomposition[1] to the time-evolution operator

$$
\begin{aligned}
S(\tau_l + \Delta\tau, \tau_l) &= e^{\tau_l H_0} e^{\Delta\tau H_0} e^{-\Delta\tau(H_0 + V)} e^{-\tau_l H_0} \\
&= e^{\tau_l H_0} e^{-\Delta\tau V} e^{-\tau_l H_0} + \mathcal{O}(\Delta\tau^2) \\
&= e^{-\Delta\tau V(\tau_l)} + \mathcal{O}(\Delta\tau^2).
\end{aligned}
\tag{2.8}
$$

But if we now try to put S back together for a finite time interval we cannot proceed further than

$$
S(\tau_f, \tau_i) = \prod_{\tau_f \ldots \tau_i} e^{-\Delta\tau V(\tau_l)},
\tag{2.9}
$$

because the interaction parts $V(\tau_l)$ do not commute at different times.

This is the hour of the time ordering operator! It shall order our times τ_l from earliest to latest.

$$
\mathcal{T}\left[c_1^{(\dagger)}(\tau_1) c_2^{(\dagger)}(\tau_2) \ldots c_n^{(\dagger)}(\tau_n)\right] = \epsilon^\sigma c_{\sigma(1)}^{(\dagger)}(\tau_{\sigma(1)}) \, c_{\sigma(2)}^{(\dagger)}(\tau_{\sigma(2)}) \ldots c_{\sigma(n)}^{(\dagger)}(\tau_{\sigma(n)}),
\tag{2.10}
$$

with

$$
\tau_{\sigma(1)} \geqslant \tau_{\sigma(2)} \geqslant \ldots \geqslant \tau_{\sigma(n)}.
$$

The permutation necessary for the ordering is denoted by σ; ϵ is -1 or 1 for fermions or bosons, respectively. To make the operator bullet proof we agree on the convention that the order of concurrent creators or concurrent annihilators is preserved. Additionally, for creators and annihilators acting at the same time the creator always acts after the annihilator, $c^\dagger(\tau) = c^\dagger(\tau + 0^+)$. Now the ordering is unique. With this powerful device at hand we succeed in finding a beautiful expression for the time-evolution operator.

$$
\begin{aligned}
S(\tau_f, \tau_i) &= \prod_{\tau_f \ldots \tau_i} e^{-\Delta\tau V(\tau_l)} \\
&= \mathcal{T} \prod_{\tau_f \ldots \tau_i} e^{-\Delta\tau V(\tau_l)} \\
&= \mathcal{T} e^{-\sum \Delta\tau V(\tau_l)}
\end{aligned}
\tag{2.11}
$$

---

[1] The Trotter decomposition is $e^{\frac{1}{m}(A+B)} = e^{\frac{1}{m}A} e^{\frac{1}{m}B} + \mathcal{O}\left(\frac{1}{m^2}\right)$ and may be proved straight forwardly.

And, finally,

$$S(\tau_f, \tau_i) = \mathcal{T} e^{-\int_{\tau_i}^{\tau_f} d\tau V(\tau)}. \tag{2.12}$$

This is the famous time-ordered exponential! Appreciate how the time ordering operator elegantly resolves the problem of non-communicating operators by giving them a unique order.

Let us now have a look at the partition function and examine how the expanded time-ordered exponential helps us to evaluate it.

$$
\begin{aligned}
\frac{Z}{Z_0} &= \langle S(\beta, 0) \rangle_0 \\
&= \sum_n \frac{(-1)^n}{n!} \int_0^\beta d\tau_1 \dots \int_0^\beta d\tau_n \langle \mathcal{T} V(\tau_1) \dots V(\tau_n) \rangle_0 \\
&= \sum_n (-1)^n \int_0^\beta d\tau_1 \dots \int_0^{\tau_{n-1}} d\tau_n \sum_1 \dots \sum_n U_1 \dots U_n \\
&\quad \cdot \left\langle c_{\alpha_1}^\dagger c_{\beta_1} c_{\gamma_1}^\dagger c_{\delta_1} \dots c_{\alpha_n}^\dagger c_{\beta_n} c_{\gamma_n}^\dagger c_{\delta_n} \right\rangle_0 \\
&= \sum_{C_n} (-1)^n U_1 \dots U_n \left\langle \mathcal{T} c_{\alpha_1}^\dagger c_{\beta_1} c_{\gamma_1}^\dagger c_{\delta_1} \dots c_{\alpha_n}^\dagger c_{\beta_n} c_{\gamma_n}^\dagger c_{\delta_n} \right\rangle_0
\end{aligned} \tag{2.13}
$$

For brevity of notation we introduced $U_1 = U_{\alpha_1 \beta_1 \delta_1 \gamma_1}$, the sums summing over all possible index sets, and made the times for each and every creation and annihilation operator implicit, $c_{\alpha_1}^\dagger = c_{\alpha_1}^\dagger(\tau_1)$, et cetera. In the third line we time-ordered the operators "by hand" by choosing the integration ranges appropriately. As for each explicitly time-ordered expression we have $n!$ equivalent non-time-ordered expressions, we gain a factor of $n!$ which thus cancels. Afterwards we reintroduce the time ordering operator artificially – it doesn't hurt to time-order an already time-ordered expression. Lastly, we unite all integrals and sums in the symbolic shorthand notation $\sum_{C_n}$. Now a time-ordered expectation value of the free system $\langle \mathcal{T} \bullet \rangle_0$ allows for a Wick decomposition. The expectation value is equivalent to the total pairing of all creators and annihilators, that is, to the sum of all possible ways to combine these operators into contractions. A contraction is defined as

$$
\begin{aligned}
\overline{c_\alpha^\dagger(\tau_1) c_\beta(\tau_2)} &= \left\langle \mathcal{T} c_\alpha^\dagger(\tau_1) c_\beta(\tau_2) \right\rangle_0 \\
&= -\left\langle \mathcal{T} c_\beta(\tau_2) c_\alpha^\dagger(\tau_1) \right\rangle_0 \\
&= G_{\beta\alpha}^0(\tau_2 - \tau_1),
\end{aligned} \tag{2.14}
$$

with the free Green's function $G^0_{\beta\alpha}(\tau)$ which is homogeneous in time[2]. In most cases we assume that the number of particles is preserved in the unperturbed system H_0, thus contractions of two creators or annihilators, respectively, are zero and need not to be taken into account. As an example for the Wick decomposition, consider the second order where the total pairing will be comprised of 4! addends and will look like

$$
\begin{aligned}
\left\langle \mathcal{T} c^\dagger_{\alpha_1} c_{\beta_1} c^\dagger_{\gamma_1} c_{\delta_1} c^\dagger_{\alpha_2} c_{\beta_2} c^\dagger_{\gamma_2} c_{\delta_2} \right\rangle_0 = {} & G^0_{\beta_1\alpha_1} G^0_{\delta_1\gamma_1} G^0_{\beta_2\alpha_2} G^0_{\delta_2\gamma_2} \\
& - G^0_{\beta_2\alpha_1} G^0_{\beta_1\alpha_2} G^0_{\delta_1\gamma_1} G^0_{\delta_2\gamma_2} \\
& + \dots .
\end{aligned}
\tag{2.15}
$$

Here, again, times are implicit.

Usually, this is the starting point for diagrammatic perturbation theory where we understand the free Green's function as a propagator and identify each possible pairing of each order with a particular Feynman diagram. However, that is not the route that we will pursue here. Instead we compute the Wick-decomposed expectation value – the total pairing – by "brute force". Consider a matrix filled with all possible free Green's functions.

$$
M_{C_n} = \begin{pmatrix}
G^0_{\beta_1\alpha_1} & G^0_{\beta_1\gamma_1} & G^0_{\beta_1\alpha_2} & G^0_{\beta_1\gamma_2} & \cdots & G^0_{\beta_1\alpha_n} & G^0_{\beta_1\gamma_n} \\
G^0_{\delta_1\alpha_1} & G^0_{\delta_1\gamma_1} & G^0_{\delta_1\alpha_2} & G^0_{\delta_1\gamma_2} & \cdots & G^0_{\delta_1\alpha_n} & G^0_{\delta_1\gamma_n} \\
G^0_{\beta_2\alpha_1} & G^0_{\beta_2\gamma_1} & G^0_{\beta_2\alpha_2} & G^0_{\beta_2\gamma_2} & \cdots & G^0_{\beta_2\alpha_n} & G^0_{\beta_2\gamma_n} \\
G^0_{\delta_2\alpha_1} & G^0_{\delta_2\gamma_1} & G^0_{\delta_2\alpha_2} & G^0_{\delta_2\gamma_2} & \cdots & G^0_{\delta_2\alpha_n} & G^0_{\delta_2\gamma_n} \\
\vdots & \vdots & \vdots & \vdots & \ddots & \vdots & \vdots \\
G^0_{\beta_n\alpha_1} & G^0_{\beta_n\gamma_1} & G^0_{\beta_n\alpha_2} & G^0_{\beta_n\gamma_2} & \cdots & G^0_{\beta_n\alpha_n} & G^0_{\beta_n\gamma_n} \\
G^0_{\delta_n\alpha_1} & G^0_{\delta_n\gamma_1} & G^0_{\delta_n\alpha_2} & G^0_{\delta_n\gamma_2} & \cdots & G^0_{\delta_n\alpha_n} & G^0_{\delta_n\gamma_n}
\end{pmatrix}
\tag{2.16}
$$

The indices of the creators label the columns, the indices of the annihilators label the rows. It is easily, if laboriously, verified that the determinant of this matrix reproduces the total pairing introduced above for a given set of indices and times of a given order. We call this set a configuration C_n consisting of n vertices $\{\alpha, \beta, \gamma, \delta, \tau\}$.

$$
\left\langle \mathcal{T} c^\dagger_{\alpha_1} c_{\beta_1} c^\dagger_{\gamma_1} c_{\delta_1} \dots c^\dagger_{\alpha_n} c_{\beta_n} c^\dagger_{\gamma_n} c_{\delta_n} \right\rangle_0 = \det M_{C_n}
\tag{2.17}
$$

---

[2] Note that usually in the literature on the DDQMC algorithm ([5], [12]) the free Green's function is defined as $G^0_{\alpha\beta}(\tau) = \left\langle \mathcal{T} c^\dagger_\alpha(\tau_1) c_\beta(\tau_2) \right\rangle_0$. Which definition is used doesn't matter. It just has to be used consistently.

Putting all together we are able to express our observable as higher dimensional integrals of determinants over all configurations

$$
\begin{aligned}
\langle O(\tau) \rangle &= \frac{\langle S(\beta,\tau)O(\tau)S(\tau,0) \rangle_0}{\langle S(\beta,0) \rangle_0} \\
&= \frac{\langle \mathcal{T} S(\beta,0)O(\tau) \rangle_0}{\langle S(\beta,0) \rangle_0} \\
&= \frac{\sum_{C_n}(-1)^n U_1 \dots U_n \det O_{C_n}}{\sum_{C_n}(-1)^n U_1 \dots U_n \det M_{C_n}}.
\end{aligned}
\tag{2.18}
$$

We have introduced a second matrix O_{C_n} which is quite similar to M_{C_n} except that we must add a column for each creator and a row for each annihilator of the observable. For example, to calculate the full Green's function

$$
G_{\beta\alpha}(\tau) = -\left\langle \mathcal{T} c_\beta(\tau)c_\alpha^\dagger(0) \right\rangle
\tag{2.19}
$$

at a fixed time τ we would add a column $(G^0_{\beta_1\alpha}(\tau_1), G^0_{\delta_1\alpha}(\tau_1), G^0_{\beta_2\alpha}(\tau_2), \dots)^T$ and a row $(G^0_{\beta\alpha_1}(\tau-\tau_1), G^0_{\beta\gamma_1}(\tau-\tau_1), G^0_{\beta\alpha_2}(\tau-\tau_2), \dots)$ to the matrix M_{C_n} to obtain O_{C_n}.

Stepping back and looking at what we've done so far we recognise that we have managed to put the numerically quite abstract notion of total pairing into a readily computable determinant of a matrix of free Green's functions whose values we know for every given configuration. This configuration determinant gets to the heart of the DDQMC method. True, we're still left with two admittedly very ugly integrals, but let us see if we can't tackle them with some statistical, that is, Monte Carlo methods.

2.2   A WORD ABOUT MONTE CARLO METHODS

Generally, Monte Carlo methods encompass a vast and rather diverse set of methods which share their statistical nature and reliance on computational resources. They characteristically employ pseudo random numbers to "simulate" a random experiment. In this section we will concern ourselves with the Monte Carlo integration method. We shall not attempt a mathematically stringent treatment, the reader is referred to [13] for details.

The underlying idea of Monte Carlo integration is simple.

$$
\int dx\, f(x) = \int dx\, w(x)\frac{f(x)}{w(x)} = \frac{1}{N}\sum_{x_t}\frac{f(x_t)}{w(x_t)}
\tag{2.20}
$$

Here we have rewritten the integral over an arbitrary function $f(x)$ to an integral over a weight $w(x)$ with $w(x) \geqslant 0$ and $\int dx\, w(x) = 1$ and the remaining part. By virtue of the central limit theorem this integral can be approximated by a sum over x_t, where the x_t follow the probability distribution $w(x)$. The approximation will become exact in the $N \to \infty$ limit provided that the individual x_t are uncorrelated.

We can readily apply this idea to the integrals appearing in our observable, eq. (2.18).

$$
\begin{aligned}
\langle O(\tau) \rangle &= \frac{\langle \mathcal{T}\, S(\beta, 0) O(\tau) \rangle_0}{\langle S(\beta, 0) \rangle_0} \\
&= \frac{\sum_{C_n} (-1)^n U_1 \ldots U_n \det O_{C_n}}{\sum_{C_n} (-1)^n U_1 \ldots U_n \det M_{C_n}} \\
&= \frac{\sum_{C_n} (-1)^n U_1 \ldots U_n \det M_{C_n} \cdot \left(\frac{\det O_{C_n}}{\det M_{C_n}} \right)}{\sum_{C_n} (-1)^n U_1 \ldots U_n \det M_{C_n} \cdot 1} \\
&= \frac{\sum_{C_n} w_{C_n} \cdot \langle\langle O \rangle\rangle_{C_n}}{\sum_{C_n} w_{C_n} \cdot 1}
\end{aligned}
\tag{2.21}
$$

and we will "measure" the quantity $\langle\langle O \rangle\rangle_{C_n}$ for a set of N configurations distributed according to w_{C_n}. Then, as above, we approximate O by

$$
\begin{aligned}
\langle O \rangle &= \frac{\frac{1}{N} \sum_{i=1}^{N} \langle\langle O \rangle\rangle_i}{\frac{1}{N} \sum_{i=1}^{N} 1} \\
&= \frac{1}{N} \sum_{i=1}^{N} \langle\langle O \rangle\rangle_i
\end{aligned}
\tag{2.22}
$$

One problem that is immediately apparent is that while we can easily normalise w_{C_n} as it similarly appears in the numerator and denominator, it is a priori not clear whether it is non-negative. In fact it can very well become negative. This is the infamous sign problem of fermionic quantum Monte Carlo methods! It has to be discussed and evaluated for each problem separately and we will see later on that it is non-existent for the Anderson model that we employ. However, it is crucial to keep in mind that the sign problem can be the downfall of the whole DDQMC method. That is, if the physical problem you're investigating exhibits the sign problem, DDQMC is not the way to go.

Note that the sign problem does not stop us from using a Monte Carlo integration. We can solve it formally within the context of this method by taking the absolute

value of the weight and putting the sign of the weight into the measured observable. Going back to equation (2.21) we write

$$
\begin{aligned}
\langle O(\tau) \rangle &= \frac{\sum_{C_n} w_{C_n} \cdot \langle\langle O \rangle\rangle_{C_n}}{\sum_{C_n} w_{C_n} \cdot \quad 1} \\
&= \frac{\sum_{C_n} |w_{C_n}| \cdot \langle\langle O \rangle\rangle_{C_n}}{\sum_{C_n} |w_{C_n}| \cdot \mathrm{sgn}(w_{C_n})}
\end{aligned}
\tag{2.23}
$$

where we redefined $\langle\langle O \rangle\rangle_{C_n} \to \langle\langle O \rangle\rangle_{C_n} \cdot \mathrm{sgn}(w_{C_n})$ and now measure the sign $\mathrm{sgn}(w_{C_n})$ along with $\langle\langle O \rangle\rangle$. Eq. (2.22) becomes

$$
\langle O \rangle = \frac{\sum_{i=1}^{N} \langle\langle O \rangle\rangle_i}{\sum_{i=1}^{N} \mathrm{sgn}_i}
\tag{2.24}
$$

In the absence of the sign problem the average sign $\langle \mathrm{sgn} \rangle$ will be one and we recover the original formulation (2.22). In the worst case scenario we will have $\langle \mathrm{sgn} \rangle \sim 0$ with maximal sign fluctuations. These fluctuations will yield a very large error for the observable $\langle O \rangle$, effectively making the method – while still realisable – again, worthless for the problem at hand.

We evaluate the sum in eq. (2.20), or more concretely eq. (2.23), by walking through phase space from one configuration x_t to the next configuration x_{t+1} in a manner that recovers the original distribution $w(x)$, i.e. we spend more time in the more probable configurations. Each step shall have knowledge only about the previous one – there's no memory – so that the x_t build a so-called Markov chain. Commonly, t is called the Monte Carlo time and we can associate with each time t a distribution $w_t(x)$ that attaches a probability to every configuration at this given time. Clearly these distributions evolve with time and we describe their evolution by a transition matrix $T_{y,x}$. The transition matrix must not be time dependent, if we do not want to introduce a memory.

$$
w_{t+1}(y) = \sum_x T_{y,x} w_t(x)
\tag{2.25}
$$

From the fact that w_t should stay a probability distribution at all times we derive the conditions $T_{y,x} \geqslant 0$ and $\sum_y T_{y,x} = 1$ for the transition matrix. Furthermore, it seems reasonable to require that we should be able to reach every point in phase space, if we want to recover our original distribution $w(x)$. We call this property *ergodicity*.

$$
T_{y,x}^n > 0 \qquad \text{for all } y, x \text{ and any } n
\tag{2.26}
$$

When at one point in time we have reached $w(x)$ it is surely desirable to stay within this distribution as it is the distribution we're aiming for. That's our second intuitive condition, coined *stationarity*.

$$\sum_x T_{y,x} w(x) = w(y) \tag{2.27}$$

Indeed, it can be shown [13] that with these two requirements – ergodicity and stationarity – the Monte Carlo process will reproduce the original probability distribution and thus also the integral in eq. (2.20) as the time goes to infinity. A condition which is mostly equivalent to stationarity but easier to handle in practice is the *detailed balance*.

$$T_{y,x} w(x) = T_{x,y} w(y) \tag{2.28}$$

To be more precise detailed balance assures stationarity (which we verify by summing over x in the above equation) whereas the reverse is not true in general.

Now let us embark on the task of finding a concrete transition matrix $T_{y,x}$. We try to fulfil the two conditions ergodicity and stationarity by splitting each update step in two parts.

$$T_{y,x} = T_{y,x}^0 a_{y,x} \tag{2.29}$$

First we will propose a new configuration in a way that ensures ergodicity, then we will accept or deny this configuration so as to keep the detailed balance. In practice we can "move" to a new configuration in a variety of ways

$$T_{y,x}^0 = \sum_i p_i T_i^0 \tag{2.30}$$

where we understand that each move T_i^0 covers a part of the complete transition matrix. Usually, we have no stringent proof that the resulting transition matrix $T_{y,x}^0$ really is ergodic – we just have to test it. For the DDQMC method the minimal set of moves that has been seen to ensure ergodicity includes the addition and removal of a vertex $\{\tau, \alpha, \beta, \gamma, \delta\}$. Other possible moves are the addition or removal of multiple vertices in one update step as well as moving a vertex in time, space (should the indices include a space coordinate) or Ising spin (see section 3.2). As we will observe in the next section, the p_i can then be used to tune the Monte Carlo process. Of course, we require $\sum_i p_i = 1$.

For each update move we have to fulfil the detailed balanced by accepting or denying the move. The *Metropolis scheme* chooses the acceptance rate as

$$a_{y,x} = \min \left(\frac{T^0_{x,y} w(y)}{T^0_{y,x} w(x)}, 1 \right) . \tag{2.31}$$

We confirm that the detailed balance is indeed obeyed by directly evaluating eq. (2.28) with $T_{y,x} = T^0_{y,x} a_{y,x}$ and the above $a_{y,x}$.

As an example let us look at the simplest possible case, a process that only includes the addition and removal of one vertex. Then

$$T^0_{y,x} = p_{C_{n+1},C_n} T^0_{C_{n+1},C_n} + p_{C_n,C_{n+1}} T^0_{C_n,C_{n+1}} \tag{2.32}$$

with

$$T^0_{C_n,C_{n+1}} = \frac{1}{n+1} \tag{2.33}$$

as we have to choose 1 of $n+1$ vertices for the vertex removal. For the vertex addition move it is

$$T^0_{C_{n+1},C_n} = \frac{1}{\beta} \frac{1}{N_{\alpha,\beta,\gamma,\delta}} . \tag{2.34}$$

Here we account for the fact that we have to choose a time in the range from 0 to β. $N_{\alpha,\beta,\gamma,\delta}$ denotes the number of possible index sets from which we choose one for the newly proposed configuration. Now the acceptance rate for the addition of a vertex will be

$$a_{C_{n+1},C_n} = \min \left(\frac{p_{C_n,C_{n+1}} T^0_{C_n,C_{n+1}} w_{C_{n+1}}}{p_{C_{n+1},C_n} T^0_{C_{n+1},C_n} w_{C_n}}, 1 \right) \tag{2.35}$$

and $a_{C_n,C_{n+1}}$ accordingly.

2.3   FAST UPDATES

The DDQMC algorithm we presented so far is feature complete and in fact works. But how efficient is it? We've talked a lot about configuration matrices in the preceding chapters. We know that we have to calculate the ratio of two determinants of these matrices for each update move and each measurement, and, frankly, calculating

determinants can be a costly business if the matrices are not terribly small. So how big are our configuration matrices? Each vertex corresponds to two columns and rows in the matrix and the number of vertices of course just corresponds to the perturbation order n of the expanded time-ordered exponential. While the definite answer will depend largely on the model and parameters employed we can at least get some tendencies and rough guidelines on how the perturbation order will behave. We consider the average of the perturbation order

$$
\begin{aligned}
\langle n \rangle &= \frac{Z_0}{Z} \langle S(\beta,0)n \rangle_0 \\
&= \frac{Z_0}{Z} \sum_n \frac{(-1)^n}{n!} n \int_0^\beta d\tau_1 \dots \int_0^\beta d\tau_n \langle V(\tau_1)\dots V(\tau_n) \rangle_0 \\
&= \frac{Z_0}{Z}(-1) \int_0^\beta d\tau \sum_n \frac{(-1)^n}{n!} \int_0^\beta d\tau_1 \dots \int_0^\beta d\tau_n \langle V(\tau_1)\dots V(\tau_n)V(\tau) \rangle_0 \\
&= -\int_0^\beta d\tau \frac{Z_0}{Z} \langle \mathcal{T} S(\beta,0) V(\tau) \rangle_0 \\
&= -\beta \langle V \rangle \\
&= -\beta \sum_{\alpha\beta\gamma\delta} U_{\alpha\beta\delta\gamma} \left\langle c_\alpha^\dagger c_\beta c_\gamma^\dagger c_\delta \right\rangle
\end{aligned}
\tag{2.36}
$$

Here we have used the fact that V is not explicitly time-dependent. Apparently, the perturbation order scales as the inverse temperature β and is also linear in the interaction parameters $U_{\alpha\beta\delta\gamma}$. The sum also suggests – and this is true quite generally – that n will increase with the system size. All in all, we expect the computation to become increasingly harder for low temperatures, large interactions and large systems.

A naïve approach to the calculation of determinants yields an order of $\mathcal{O}(n!)$, however, with the help of a LU decomposition we achieve $\mathcal{O}(n^3)$. But we can do better! We can do better with *Fast Updates*. Note how the matrices whose determinants' ratio we calculate are very similar – usually we have added, removed or changed only a few columns and rows. The obvious idea is to exploit these similarities with some clever matrix relations. It's not so obvious how exactly to do it and, although not difficult in principle, it is tricky and also a bit lengthy. The gory technical details are in appendix A, here we only state the results of this endeavour in matrix algebra. Again, we concentrate on the two principal update moves, the addition and removal of a vertex, although it should be possible to find similar relations for other moves.

Consider the two $(n+k) \times (n+k)$ matrices

$$M = \begin{pmatrix} A & B \\ C & D \end{pmatrix}, \qquad M^{-1} = \begin{pmatrix} P & Q \\ R & T \end{pmatrix}, \tag{2.37}$$

made up of $n \times n$ block matrices A and P, respectively, with B, C, D as well as Q, R and T sized accordingly. The Schur complement of the block A of matrix M is

$$S = D - CA^{-1}B. \tag{2.38}$$

Now the following statements hold.

$$\frac{\det A}{\det M} = \det T \tag{2.39}$$

$$A^{-1} = P - QT^{-1}R \tag{2.40}$$

$$\frac{\det M}{\det A} = \det S \tag{2.41}$$

$$M^{-1} = \begin{pmatrix} A^{-1} + B'S^{-1}C' & -B'S^{-1} \\ S^{-1}C' & S^{-1} \end{pmatrix} \tag{2.42}$$

For the last equation we've introduced the shorthand notation $B' = A^{-1}B$ and $C' = CA^{-1}$.

Say, we propose the addition of a vertex $\{\tau, \alpha, \beta, \gamma, \delta\}$. Looking back at the particular form of the configuration matrix (2.16) we see that the new matrix is just like the old matrix, but with two additional columns and rows. We identify the old configuration matrix M_{C_n} as A and the new matrix $M_{C_{n+1}}$ as M. The added columns and rows are put into the $(n \times 2)$ matrix B, the $(2 \times n)$ matrix C and the (2×2) matrix D. The Schur complement (2.38) is readily computed with the help of the old inverse configuration matrix $A^{-1} = M_{C_n}^{-1}$. Now eq. (2.41) yields the ratio of the determinants of the new and the old matrix and the acceptance rate (2.35) can be calculated. If the move is accepted, the new inverse configuration matrix $M^{-1} = M_{C_{n+1}}^{-1}$ may be obtained by virtue of eq. (2.42).

The removal of a vertex is the reverse operation of the vertex addition. For the sake of simplicity we assume that the vertex which is removed is the last vertex of the configuration C_n. Thus the last two columns and rows of the configuration matrix are to be removed. Should this not be the case, columns and rows can be swapped accordingly, see appendix A for details. Again, we identify the old configuration

matrix $M_{C_{n+1}}$ as M. The new configuration matrix M_{C_n} is A. It follows that eq. (2.39) allows us to compute the acceptance rate, while eq. (2.40) calculates the new inverse configuration matrix $A^{-1} = M_{C_n}^{-1}$.

Apparently, the knowledge of the inverse configuration matrix is sufficient for the vertex addition and removal operations, and hence for the DDQMC method at large. We don't need the configuration matrix itself. Empirical investigation shows that the inverse configuration matrix is very well-conditioned. No issues arise from the limited numerical precision. As a result, for practical simulation run-times, there's no need to ever rebuild the inverse configuration matrix from scratch, that is, from the bare configuration C_n.

Before we turn our attention to the efficiency of the Fast Update operations presented so far, let us shortly think about how we can carry out the measurement of an observable. As an example, we consider the Green's function $G_{\beta\alpha}(\tau)$, eq. (2.19), again. From eq. (2.21) we gather that for each measurement we must calculate the quantity $\langle\langle O(\tau)\rangle\rangle_{C_n} = \det O_{C_n}(\tau)/\det M_{C_n}$. We discussed at the end of section 2.1, that the (time-dependent) matrix $O_{C_n}(\tau)$ is just like M_{C_n}, but for an added column and row. As before, we apply relation (2.41), but this time around B and D are τ-dependent. Consequently, the calculation needs to be carried out for each and every τ-point of the Green's function. For the measurement of observables, as already for the vertex addition and removal, only the inverse configuration is required.

The computational complexity of $(2 \times n) \times (n \times n)$, $(1 \times n) \times (n \times n)$ and similar matrix multiplications is in $\mathcal{O}(n^2)$. Therefore, this is also the efficiency of the vertex addition and removal operations and, related, the measurement of an observable, as we gather from a study of the Fast Update equations (2.40), (2.41) and (2.42). Apart from determinants of (2×2) matrices, which are, of course, of constant order, they only involve such matrix multiplications. A notable exception is the proposal of a vertex removal, (2.39), that is of constant order only. Thus, proposing a vertex removal is computationally much cheaper than proposing a vertex addition. We can exploit this fact by tuning the proposal probabilities $p_{C_n,C_{n+1}}$ and p_{C_{n+1},C_n} originally introduced in eq. (2.30). We anticipate that it might be beneficial to propose the removal more often than the addition of a vertex. All in all, the Fast Updates are seen to have an upper boundary of $\mathcal{O}(n^2)$. So compared with the simpler LU decomposition with a complexity of $\mathcal{O}(n^3)$ we gain one order in efficiency.

Lastly, with updates of the order $\mathcal{O}(n^2)$ the run-time of the simulation at large will scale as $\mathcal{O}(n^3)$. The reason is that the "natural" time unit of a Monte Carlo simulation process is not a single update step, but a *sweep*. By a sweep we understand the

update of the complete configuration C_n, so roughly n update steps. Expectedly, for a simulation with a higher average perturbation order it will take longer to update the complete configuration once.

2.4   PRACTICAL IMPLEMENTATION

In the preceding sections we have described the physical as well as mathematical foundation and facets of the DDQMC method in some detail. For this last section we approach the algorithm from a more practical position, that is, from an implementer's point of view.

Suppose we have chosen a physical model of interest. It might be, for example, the one or two dimensional Hubbard model, or, as in our case, the Anderson model, which we discuss at length in the next chapter. For a given set of parameters we will then be able to calculate the free Green's function. The problem and system size permitting, it will be beneficial to make a table of the free Green's before the Monte Carlo process is started. To this end the imaginary time and, if necessary, other vertex indices are discretised. Obviously, the table will vastly improve the run-time of the simulation.

We start the Monte Carlo process with an initial configuration C_n^0. It is convenient to start with an empty configuration and hence a zero-size inverse configuration matrix as well. For an update step we choose one of the implemented update moves randomly, but according to their proposal probability p_i, see (2.30). The easiest case is to choose either the addition or removal of a vertex, each with a fifty-fifty chance. When we are adding a vertex we draw the imaginary time τ randomly from the range 0 to β, the inverse temperature, and similarly all other vertex indices. For example, for a one-dimensional Hubbard model we would additionally choose a site on the one-dimensional chain. Reversely, when we remove a vertex it is again the random number generator that decides which vertex is to be removed. The heavy reliance of the method on random numbers should now be apparent. Consequently, the choice and quality of the employed pseudo random number generator deserves some consideration. Having proposed the move, the acceptance rate is computed following the Metropolis scheme, eq. (2.35), and using the Fast Update formulas presented in the last section. If the move is accepted (again, by virtue of a random number), we compute the new inverse configuration matrix and append the new vertex to the configuration or remove the deleted vertex. Subsequently, we proceed

to the next update step. If the move is denied, well, we leave everything as it is and proceed to the next update step just the same.

After some updates we might decide to do a measurement of our observables. Typical observables include the Green's function, the perturbation order or the spin-resolved occupancy. Of course, additional observables depend largely on the physical problem under consideration. Also, some observables, like the perturbation order, are simple scalar quantities while others, like the Green's function, are functions of one or more parameters. Not surprisingly, we will discretise these parameters. For example, for the Green's function a τ-discretisation of 100 or 200 values might be a common choice. Again, we employ Fast Updates to compute the value of each observable $\langle\langle O \rangle\rangle_{C_n}$ which we store to disk, together with the sign of the weight $\text{sgn}(w_{C_n})$.

Before the first measurement is carried out, though, the system warms up. That is, we wait for the Monte Carlo process to "forget" its initial (empty) configuration. If we introduce a Monte Carlo time that counts the number of completed updates, then the duration of the initial warm-up phase is specified by the warm-up time. Naturally, the warm-up phase is expected to take longer for simulations with higher average perturbation orders. In a similar vein, for the central limit theorem to be valid, for each observable the measured values must be statistically independent. Therefore we usually measure only every 100 or 1000 update steps – to name some typical numbers. Often it is sensible to subsume a couple of measurements before the value is written to disk, so as to keep the disk usage in reasonable bounds for very large simulations. These raw data are subsequently rebinned again, i.e. we accumulate a number of succeeding measurements a second time, into a bin. Now the value of each bin is considered a genuine measurement. Depending on the problem and observable as few as 50 to 100 bins may be sufficient to yield a statistically reasonable average value for the observable. Practically, for, say, 10 to 100 million original measurements $\langle\langle O \rangle\rangle_{C_n}$ we are then pretty confident that the bin values are uncorrelated. If we want to err on the side of caution, the autocorrelation of each observable has to be calculated. The autocorrelation is expected to drop off exponentially over the Monte Carlo time. Thus we attach an autocorrelation time to each and every observable and by choosing the bin size much bigger than this autocorrelation time, we are dead sure that the values of the bins are statistically uncorrelated. They are independent. Autocorrelation times are different for different observables and as a consequence, we could choose different intervals for the measurements and rebin the raw data differently, as well – gaining better results for observables with shorter autocorrelation

times. Practically, all observables are treated the same in this regard. Also, in the common case we only check the autocorrelation occasionally.

The final value for a given observable is obtained by dividing the average of all bins by the average measured sign, which, incidentally, we accumulated and binned just like the observable itself, eq. (2.24). The error is conveniently calculated by means of the Jackknife or Bootstrap methods [14].

THE ANDERSON MODEL

We want to describe, model and ultimatively simulate a transition metal or rare earth ion embedded in a metallic host. Under appropriate conditions such an impurity is seen to exhibit a local magnetic moment and, more interesting still, the Kondo effect at low temperatures. For those systems, the outer $3d$ shell (transition metals, for example Fe) or $4f$ shell (rare earths, for example Ce) of the impurity lies within the conduction band of the host metal (might be, for example, Cu or $Mo - Nb$ alloys). Naturally, the conduction electrons are expected to scatter off the impurity ion and thus the most straight forward way is to treat the impurity simply as a scattering potential. Such an approach will yield a virtual bound state resonance in the density of states of the band electrons. However, by it's very nature the approach cannot succeed in exposing a local moment. In 1961, Anderson set out to tackle the problem in quite a different way [1]. He proposed the Hamiltonian

$$
\begin{aligned}
H &= H_{bath} + H_{d0} + H_{d1} + H_V \\
&= \sum_{k\sigma} \epsilon_k n_{k\sigma} + \sum_\sigma \epsilon_d n_{d\sigma} + U n_{d\uparrow} n_{d\downarrow} + \sum_{k\sigma} \left(V_{dk} d_\sigma^\dagger c_{k\sigma} + V_{kd} c_{k\sigma}^\dagger d_\sigma \right) .
\end{aligned}
\tag{3.1}
$$

Here, the impurity is modelled similar to an atomic state. This is justified, because the d or f shells tend to be very strongly localised. The energy of such a shell is ϵ_d and $d^\dagger$ and d create or annihilate an electron on the impurity, respectively. It is the simplest case that we capture with the term H_{d0}: the singular non-degenerate orbital. H_{bath} describes the host metal – the bath – the impurity is embedded in. The conduction band electrons are created in a Bloch state $|k\rangle$ by $c_k^\dagger$, they are annihilated by c_k. Their dispersion relation is denoted by ϵ_k. Anderson originally used a flat band assumption for the bath, but, of course, a tight-binding approach can be employed equally. The interplay of the impurity and the host metal is introduced by the hybridisation part H_V, also sometimes referred to as s-d interaction term. It describes the "hopping" of electrons from a Bloch state to the localised d-state of the impurity ion and vice versa, by virtue of the hybridisation or overlap constants V_{dk} and V_{kd}. Lastly, we include a Coulomb-interaction on the impurity, H_{d1}, and only on the impurity. Here, due to

the strong localisation of the shell, the electron-electron interaction is expected to be large. In contrast, for the delocalised bath electrons it can be neglected.

Anderson has argued that the impurity state $|d\rangle$ and the Wannier states of the bath $|i\rangle$ (and consequently the Bloch states of the bath $|k\rangle$) can be approximately treated as being orthogonal. Contributing bath electrons are mostly from s or p orbitals whereas the impurity is a d or f orbital. Thus, for symmetry reasons we expect $\langle d|i\rangle \sim 0$. In that sense $|d\rangle$ and $|i\rangle$ are base kets for our problem.

The Hamiltonian of the Anderson model introduced above can be extended to multiple impurities within a host metal and is then referred to as the periodic Anderson model (PAM). Not surprisingly, the "simple" Hamiltonian we're using here is termed the single impurity Anderson model (SIAM). If we omit the interaction term H_{d1} it's called the non-interacting Anderson model. A further distinction in terminology is made with respect to the impurity level ϵ_d. We have the symmetric Anderson model for $\epsilon_d = 0$ and, conversely, the asymmetric Anderson model for $\epsilon_d \neq 0$. Finally, it is remarkable that the simple Hamiltonian proposed by Anderson does not only, as expected, reproduce the virtual bound state resonance of the simple scattering potential, but is also sufficient to expose a local moment and, as we will see later on, the Kondo effect.

3.1   LOCAL HYBRIDISATION

We gain a physically very intuitive picture if we take the conduction band electrons from k- to real space. Let $c_i^\dagger$ create an electron and c_i annihilate an electron in a Wannier state $|i\rangle$. From now on we shall consider a one-dimensional system exclusively, where i numbers the sites of a chain and we choose periodic boundary conditions. For the bath and hybridisation term we write

$$
\begin{aligned}
H_{bath} + H_V &= \sum_k \epsilon_k n_k + \sum_k \left(V_{dk} d^\dagger c_k + V_{kd} c_k^\dagger d \right) \\
&= \sum_{i,j} t_{i,j} c_i^\dagger c_j + \sum_{i,j} \left(V_{di} d^\dagger c_i + V_{jd} c_j^\dagger d \right) .
\end{aligned}
\tag{3.2}
$$

Here we have made all spins implicit. Usually, a tight-binding approximation is applied to the overlap integral $t_{i,j}$.

$$
t_{i,j} = \langle i| H |j\rangle \, \delta_{j,i\pm1} = \langle i| H |i\pm1\rangle \, \delta_{j,i\pm1} = -t \, \delta_{j,i\pm1}
\tag{3.3}
$$

Thus we allow only for next-neighbour hopping. In a similar spirit we assume for the hybridisation

$$V_{di} = \langle d| H |i\rangle \, \delta_{i,0} = \langle d| H |0\rangle \, \delta_{i,0} = V \, \delta_{i,0} \,, \tag{3.4}$$

$$V_{id} = \langle i| H |d\rangle \, \delta_{i,0} = \langle 0| H |d\rangle \, \delta_{i,0} = V^* \, \delta_{i,0} \,, \tag{3.5}$$

where $|0\rangle$ denotes the first site of the bath. This is the local hybridisation approximation! Note that in contrast to t which is purely real for symmetry reasons, the hybridisation V a-priori is not. However, we can make it real by absorbing the phase of V and V^* into the impurity state $\langle d|$ and $|d\rangle$ in the above equations, respectively. Changing the phase of the d-state leaves the physics invariant, it's a canonical transformation. Now we can rewrite eq. (3.2).

$$H_{bath} + H_V = -t \sum_{\langle i,j\rangle} c_i^\dagger c_j + V d^\dagger c_0 + V c_0^\dagger d \,. \tag{3.6}$$

The interpretation of our Hamiltonian becomes obvious. It describes an impurity with an adjacent bath in the form of a one-dimensional chain. In the chain electrons can hop from one lattice site to the next with a hopping parameter t. Additionally, we have hopping to and from the impurity with a hopping parameter V, which we coined the hybridisation parameter. Going back to k-space, which is more convenient for computation, we have the well-known cosine dispersion relation for the nearest-neighbour hopping

$$\epsilon_k = -2t \cos(k) \,, \tag{3.7}$$

using a lattice constant of unity. The hybridisation parameter becomes

$$V_{dk} = \langle d| H |k\rangle = \sum_j \frac{1}{\sqrt{N}} e^{ikj} \langle d| H |j\rangle = \frac{1}{\sqrt{N}} V e^{ik\cdot 0} = \frac{V}{\sqrt{N}} \tag{3.8}$$

$$V_{kd} = \langle k| H |d\rangle = \sum_j \frac{0}{\sqrt{N}} e^{-ikj} \langle j| H |d\rangle = \frac{1}{\sqrt{N}} V e^{-ik\cdot 0} = \frac{V}{\sqrt{N}} \tag{3.9}$$

Finally, for the complete Anderson Hamiltonian we write

$$\begin{aligned} H &= H_{bath} + H_{d0} + H_{d1} + H_V \\ &= \sum_k \epsilon_k n_k + \epsilon_d n_d + U n_{d\uparrow} n_{d\downarrow} + \frac{V}{\sqrt{N}} \sum_k \left(d^\dagger c_k + c_k^\dagger d \right) \,. \end{aligned} \tag{3.10}$$

Again, to ease notation spins are implicit unless written down explicitly.

3.2   APPLYING THE DDQMC METHOD

Having stated the Hamiltonian for the Anderson impurity which we want to investigate, we are now in a position to apply the DDQMC method developed in the last chapter. We laid out the algorithm for a very general Hamiltonian of the form

$$H = H_0 + V = \sum_{\alpha\beta} t_{\alpha\beta} c_\alpha^\dagger c_\beta + \sum_{\alpha\beta\gamma\delta} U_{\alpha\beta\delta\gamma} c_\alpha^\dagger c_\beta c_\gamma^\dagger c_\delta \,. \tag{3.11}$$

For our Hamiltonian (3.10) we readily identify the interacting part $V = H_{d1}$ and the non-interacting part $H_0 = H_{bath} + H_{d0} + H_V$. In section 2.2 we noted the necessity of checking the sign problem for each physical problem separately. Furthermore, we observed that the sign problem can be the downfall of the DDQMC method at large. Here we are with our particular problem. Before everything else, let us check how the Anderson model fares with respect to the sign problem.

To this end we evaluate the weight w_{C_n} introduced in equation (2.21). Together with eq. (2.17) and our interaction term H_{d1} we write for the weight

$$\begin{aligned} w_{C_n} &= (-1)^n U^n \det M_{C_n} \\ &= (-U)^n \left\langle \mathcal{T} n_{d\uparrow}(\tau_1) n_{d\downarrow}(\tau_1) \dots n_{d\uparrow}(\tau_n) n_{d\downarrow}(\tau_n) \right\rangle_0 \,. \end{aligned} \tag{3.12}$$

Going back one step further, we remember how the weight emerged from the time-ordered exponential, (2.12). For the Anderson impurity it becomes

$$\left\langle S(\beta, 0) \right\rangle_0 = \left\langle \mathcal{T} e^{-\int_0^\beta d\tau U n_{d\uparrow}(\tau) n_{d\downarrow}(\tau)} \right\rangle_0 \,. \tag{3.13}$$

As the exponential is expanded, the sign of the exponent yields the sign of the weight w_{C_n} for each order. In our model we employ a repulsive interaction $U > 0$. Thus we are pretty confident to assert that the integral

$$\int_0^\beta d\tau \, U n_{d\uparrow}(\tau) n_{d\downarrow}(\tau) \tag{3.14}$$

is positive on average. The overall sign of the exponent is negative and the sign of the weight alternates from one order to the next. This is the worst-case sign problem. The average sign is zero, $\langle \mathrm{sgn} \rangle \sim 0$.

In an attempt to improve the situation we rewrite the Hubbard term

$$H_{d1} = U \left(n_{d\uparrow} - \frac{1}{2} \right) \left(n_{d\downarrow} - \frac{1}{2} \right) \,. \tag{3.15}$$

This step renormalises ϵ_d, $\epsilon_d \to \epsilon_d - \frac{1}{2}U$, and adds a constant $\frac{1}{4}$ to the Hamiltonian. Well, constants can always be safely ignored[1] and the redefinition of ϵ_d only shifts the impurity levels. It leaves the physics untouched. Still, we have to keep the redefinition in mind when discussing the levels of the impurity. We consider the integral in the exponent again.

$$\int_0^\beta d\tau\, U \left(n_{d\uparrow}(\tau) - \frac{1}{2} \right) \left(n_{d\downarrow}(\tau) - \frac{1}{2} \right) \tag{3.16}$$

Now at least at half-filling where the impurity mostly carries either an up or down spin, the integral is expected to be negative on average. Consequently, the sign of the weight will be positive.

To get a grip on the sign problem when we're at a different filling factor we rewrite the interaction term a second time. We introduce a dynamical Ising field.

$$H_{d1} = \frac{U}{2} \sum_{s=\pm 1} \left(n_{d\uparrow} - \alpha_\uparrow(s) \right) \left(n_{d\downarrow} - \alpha_\downarrow(s) \right) \tag{3.17}$$

with

$$\alpha_\sigma(s) = \frac{1}{2} + \sigma s \delta \tag{3.18}$$

The original Hamiltonian is recovered apart from a constant δ^2. The newly implemented Ising spin is denoted by s and δ is a tunable parameter which we choose to be $\delta = 0.5 + 0^+$. The electron spin is $\sigma = \pm 1$. We turn our attention to the integral a last time.

$$\sum_{s=\pm 1} \int_0^\beta d\tau\, \frac{U}{2} \left(n_{d\uparrow}(\tau) - \alpha_\uparrow(s) \right) \left(n_{d\downarrow}(\tau) - \alpha_\downarrow(s) \right) \tag{3.19}$$

It is easily verified that for all possibilities, the impurity being vacated, singly or doubly occupied, the above expression is always negative with the aforementioned choice of δ. Hence the sign problem effectively disappears.

Note that although the reasoning presented so far is more of a handwaving nature, it is correct in essence. The Anderson impurity does not exhibit the sign problem.

---

1 Constant terms in the Hamiltonian resurface as constant factors in the partition function. Therefore they cancel in expectation values, for example eq. (2.2), where they appear in the numerator as well as in the denominator.

An extended and more precise study [12] establishes the related one-dimensional Hubbard model as another physical problem that does not suffer from a vanishing average sign. Conversely, this is no longer the case when we go from the one-dimensional to the two-dimensional Hubbard model, which, in general, is subject to the sign problem.

With the newly established interaction term H_{d1}, let us now state the complete Hamiltonian of the Anderson model in the form that we are putting to use for the DDQMC algorithm.

$$
\begin{aligned}
H = \sum_{k\sigma} \epsilon_k n_{k\sigma} &+ \sum_\sigma \epsilon_d n_{d\sigma} + \frac{V}{\sqrt{N}} \sum_{k\sigma} \left(d^\dagger_\sigma c_{k\sigma} + c^\dagger_{k\sigma} d_\sigma \right) \\
&+ \frac{U}{2} \sum_{s=\pm 1} \left(n_{d\uparrow} - \alpha_\uparrow(s) \right) \left(n_{d\downarrow} - \alpha_\downarrow(s) \right)
\end{aligned}
\tag{3.20}
$$

The non-interacting part of the Hamiltonian is diagonal with respect to the spin projection, it cannot flip spins. Consequently, for the free Green's function $G^0_{\sigma\sigma'}(\tau) = -\left\langle \mathcal{T} c_\sigma(\tau) c^\dagger_{\sigma'}(0) \right\rangle_0$ we will have $G^0_{\uparrow\downarrow} = G^0_{\downarrow\uparrow} = 0$. Also, $G^0_{\uparrow\uparrow} = G^0_{\downarrow\downarrow}$. So the free Green's function is basically spin independent,

$$
G^0(\tau) = -\left\langle \mathcal{T} c(\tau) c^\dagger(0) \right\rangle_0 ,
\tag{3.21}
$$

and we will see how we can calculate this quantity in a minute, in the next section. The spin-independence has a bearing on the determinant of the configuration matrix (2.17) as well: The determinant factorises. This is easiest understood by keeping in mind that contractions (which are precisely the free Green's functions) between creators and annihilators of opposite spin now vanish. Instead of one configuration matrix we get two, one for each spin.

$$
\begin{aligned}
\det M_{C_n} &= \left\langle \mathcal{T} \left(n_\uparrow(\tau_1) - \alpha_\uparrow(s_1) \right) \left(n_\downarrow(\tau_1) - \alpha_\downarrow(s_1) \right) \cdot \right. \\
&\qquad \left. \dots \cdot \left(n_\uparrow(\tau_n) - \alpha_\uparrow(s_n) \right) \left(n_\downarrow(\tau_n) - \alpha_\downarrow(s_n) \right) \right\rangle_0 \\
&= \left\langle \mathcal{T} \left(n_\uparrow(\tau_1) - \alpha_\uparrow(s_1) \right) \dots \left(n_\uparrow(\tau_n) - \alpha_\uparrow(s_n) \right) \right\rangle_0 \\
&\qquad \cdot \left\langle \mathcal{T} \left(n_\downarrow(\tau_1) - \alpha_\downarrow(s_1) \right) \dots \left(n_\downarrow(\tau_n) - \alpha_\downarrow(s_n) \right) \right\rangle_0 \\
&= \det M_{C_n\uparrow} \det M_{C_n\downarrow}
\end{aligned}
\tag{3.22}
$$

Notice that we do the sum over the Ising spins s_l by the Monte Carlo process as well, just as the integrals over the imaginary time. Thus for the Anderson impurity the

configuration C_n consists of n rather simple vertices $\{s, \tau\}$. The configuration matrix takes the form

$$M_{C_n\sigma} = \begin{pmatrix} G^0(0) - \alpha_\sigma(s_1) & G^0(\tau_1 - \tau_2) & \dots & G^0(\tau_1 - \tau_n) \\ G^0(\tau_2 - \tau_1) & G^0(0) - \alpha_\sigma(s_2) & \dots & G^0(\tau_2 - \tau_n) \\ \vdots & \vdots & \ddots & \vdots \\ G^0(\tau_n - \tau_1) & G^0(\tau_n - \tau_2) & \dots & G^0(0) - \alpha_\sigma(s_n) \end{pmatrix}. \tag{3.23}$$

For the sake of completeness, we state the concrete form of the Metropolis acceptance rates (2.31). A vertex addition move is accepted with the probability

$$a_{C_{n+1}, C_n} = \min\left(-\frac{U\beta}{n+1} \frac{\det M_{C_{n+1}\uparrow} \det M_{C_{n+1}\downarrow}}{\det M_{C_n\uparrow} \det M_{C_n\downarrow}}, 1 \right) \tag{3.24}$$

and, reversely, the acceptance rate for the removal of a vertex is

$$a_{C_n, C_{n+1}} = \min\left(-\frac{n+1}{U\beta} \frac{\det M_{C_n\uparrow} \det M_{C_n\downarrow}}{\det M_{C_{n+1}\uparrow} \det M_{C_{n+1}\downarrow}}, 1 \right). \tag{3.25}$$

We propose both moves with the same probability, $p_{C_n, C_{n+1}} = p_{C_{n+1}, C_n} = \frac{1}{2}$.

Lastly, we note that the expectation value of the perturbation order (2.36) now reads

$$\langle n \rangle = -\beta U \left[\left\langle \left(n_{d\uparrow} - \frac{1}{2} \right) \left(n_{d\downarrow} - \frac{1}{2} \right) \right\rangle - \delta^2 \right] \tag{3.26}$$

Apparently the perturbation order depends on the parameter δ introduced above. That's why we choose δ as small as possible. In practice this means $\delta = 0.51$ generally and $\delta = 0.1$ for $\epsilon_d = 0$, at half-filling[2].

3.3 FREE GREEN'S FUNCTION

For the DDQMC method we need to make a table of the free Green's function on the impurity, $G_{dd}(\tau) = -\langle \mathcal{T} d(\tau) d^\dagger(0) \rangle_0$. The free or non-interacting part of our Hamiltonian is

$$\begin{aligned} H_{ni} &= \sum_k \epsilon_k c_k^\dagger c_k + \epsilon_d d^\dagger d + \frac{V}{\sqrt{N}} \sum_k \left(d^\dagger c_k + c_k^\dagger d \right) \\ &= \sum_{i,j} T_{i,j} c_i^\dagger c_j \qquad \text{with} \, |i\rangle = |d\rangle, |k_1\rangle, |k_2\rangle, \dots. \end{aligned} \tag{3.27}$$

---

2 We cannot set $\delta = 0$ at half-filling as the weight would then vanish for odd perturbation orders, rendering the method useless [12].

We can apply the Resolvent Green's function formalism (appendix B). Eq. (B.3) states

$$\mathbf{G}(i\omega_m) = (i\omega_m - \mathbf{T})^{-1} \tag{3.28}$$

which we rewrite

$$(i\omega_m - \mathbf{T})\,\mathbf{G}(i\omega_m) = \mathbf{1} \tag{3.29}$$

The matrix elements of $\mathbf{T}$ and $\mathbf{G}$ are $\langle d|\,H\,|d\rangle$, $\langle d|\,H\,|k\rangle$, $\langle k|\,H\,|d\rangle$, $\langle k|\,H\,|k\rangle$ and G_{dd}, G_{dk}, G_{kd}, G_{kk}, respectively. This set of equations is readily solved and we obtain

$$G_{dd}(i\omega_m) = \frac{1}{i\omega_m - \epsilon_d - \frac{V^2}{N}\sum_k \frac{1}{i\omega_m - \epsilon_k}}\,. \tag{3.30}$$

For a one-dimensional chain the k-sum in (3.30) runs over N k-values where N is the number of sites of the chain. We usually employ the tight-binding approximation and therefore the dispersion relation is

$$\epsilon_k = -2t\cos(k)\,. \tag{3.31}$$

The lattice constant has been set to unity. It is usually desirable to make the size of the bath infinite and for practical purposes this means $N = 10^3\ldots10^4$. At the centre of the band the cosine band can be approximated with a flat band with the density of states $\rho = \frac{1}{W}$, W the bandwidth. In this case, the dispersion relation is

$$\epsilon_k = \frac{W}{2\pi}k \tag{3.32}$$

and the k-sum can be computed analytically.

$$
\begin{aligned}
\frac{V^2}{N}\sum_k \frac{1}{i\omega_m - \epsilon_k} &= \frac{V^2}{N}\frac{N}{2\pi}\sum_k \Delta k\frac{1}{i\omega_m - \epsilon_k} \\
&= \frac{V^2}{2\pi}\int_0^{2\pi} dk\,\frac{1}{i\omega_m - \epsilon_k} \\
&= \frac{V^2}{2\pi}\frac{2\pi}{W}\int_{-\frac{W}{2}}^{\frac{W}{2}} d\epsilon\,\frac{1}{i\omega_m - \epsilon_k} \\
&= \frac{V^2}{W}\ln\frac{i\omega_m + \frac{W}{2}}{i\omega_m - \frac{W}{2}}
\end{aligned}
\tag{3.33}
$$

So all in all we have for a flat band

$$G_{dd}(i\omega_m) = \frac{1}{i\omega_m - \epsilon_d - \frac{V^2}{W} \ln \frac{i\omega_m + \frac{W}{2}}{i\omega_m - \frac{W}{2}}}.$$

(3.34)

Now a Fourier transform yields the Green's function in imaginary time.

$$G_{dd}(\tau) = \frac{1}{\beta} \sum_{\omega_m} G(i\omega_m) e^{-i\omega_m \tau}$$

(3.35)

We will do the sum numerically, cutting off at a suitably chosen m_{max}. However, there's a neat trick that makes the sum converge faster, drastically lowering the number of addends required for a satisfyingly smooth and precise $G_{dd}(\tau)$. Quite generally, it can be shown [15] that the asymptotic behaviour of the Green's function is

$$G_{dd}(i\omega_m) = \frac{1}{i\omega_m}, \quad \text{for } |i\omega_m| \to \infty$$

(3.36)

and the Fourier transform of $\frac{1}{i\omega_m}$ can be computed analytically to

$$\frac{1}{\beta} \sum_{\omega_m} \frac{1}{i\omega_m} e^{-i\omega_m \tau} = -\frac{1}{2}\theta(\tau) + \frac{1}{2}\theta(-\tau).$$

(3.37)

Consequently, the Green's function may be written

$$G_{dd}(\tau) = \frac{1}{\beta} \sum_{\omega_m} \left(G_{dd}(i\omega_m) - \frac{1}{\omega_m} \right) e^{-i\omega_m \tau} - \frac{1}{2}\theta(\tau) + \frac{1}{2}\theta(-\tau).$$

(3.38)

In practice, 10^3 to 10^4 summands are seen to be sufficient for typical parameters and with a time-discretisation of 10^4 to 10^5 τ-points we're ready to fill our free Green's function table.

3.4 PARTICLE-HOLE TRANSFORMATION

It is instructive to investigate our problem under a particle-hole transformation. To this end we introduce the canonical transformations

$$d^\dagger = -\tilde{d}, \quad d = -\tilde{d}^\dagger,$$

(3.39)

$$c_i^\dagger = (-1)^i \tilde{c}_i, \quad c_i = (-1)^i \tilde{c}_i^\dagger.$$

(3.40)

The occupancy operator becomes

$$n_d = d^\dagger d = (-\tilde{d})(-\tilde{d}^\dagger) = 1 - \tilde{d}^\dagger \tilde{d} = 1 - \tilde{n}_d \, , \tag{3.41}$$

and similar for n_i. This illustrates the name – a particle transforms into a hole and vice versa. Let us now look at the Hamiltonian (3.20) which we write, again, in real space. As before, spins are implicit unless explicitly written down. Also note, that for our discussion here the Ising spins need not be included.

$$
\begin{aligned}
H &= \sum_k \epsilon_k c_k^\dagger c_k + \epsilon_d n_d + U(n_{d\uparrow} - \tfrac{1}{2})(n_{d\downarrow} - \tfrac{1}{2}) + \frac{V}{\sqrt{N}} \sum_k \left(d^\dagger c_k + c_k^\dagger d \right) \\
&= -t \sum_{\langle i,j \rangle} c_i^\dagger c_j + \epsilon_d n_d + U(n_{d\uparrow} - \tfrac{1}{2})(n_{d\downarrow} - \tfrac{1}{2}) + V \left(d^\dagger c_0 + c_0^\dagger d \right) \\
&= -t \sum_{\langle i,j \rangle} (-1)^i (-1)^j \tilde{c}_i \tilde{c}_j^\dagger + \epsilon_d(1 - \tilde{n}_d) + U(1 - \tilde{n}_{d\uparrow} - \tfrac{1}{2})(1 - \tilde{n}_{d\downarrow} - \tfrac{1}{2}) \\
&\quad + V \left(-\tilde{d} \tilde{c}_0^\dagger - \tilde{c}_0 \tilde{d}^\dagger \right) \\
&= -t \sum_{\langle i,j \rangle} \tilde{c}_j^\dagger \tilde{c}_i + \epsilon_d - \epsilon_d \tilde{n}_d + U(\tilde{n}_{d\uparrow} - \tfrac{1}{2})(\tilde{n}_{d\downarrow} - \tfrac{1}{2}) + V \left(\tilde{c}_0^\dagger \tilde{d} + \tilde{d}^\dagger \tilde{c}_0 \right)
\end{aligned}
\tag{3.42}
$$

Apparently, the Hamiltonian is invariant under a particle-hole transformation for $\epsilon_d = 0$. Appreciate how the invariance is linked to the sign problem. While the new form of the interaction term $U(n_{d\uparrow} - \tfrac{1}{2})(n_{d\downarrow} - \tfrac{1}{2})$ is invariant under the transformation, the original term $U n_{d\uparrow} n_{d\downarrow}$ is not. Remember that it was the original form that caused the worst-case sign $\langle \text{sgn} \rangle = 0$. Lastly, as the singular constant term ϵ_d bears no relevance for the Hamiltonian and thus the problem at large, we acknowledge that the particle-hole transformation for $\epsilon_d \neq 0$ simply corresponds to changing the sign of ϵ_d, $\epsilon_d \rightarrow -\epsilon_d$.

We investigate the spin susceptibility

$$
\begin{aligned}
\chi_s &= \int_0^\beta d\tau \, \langle s(\tau) s(0) \rangle = \int_0^\beta d\tau \, \left\langle \left(n_{d\uparrow}(\tau) - n_{d\downarrow}(\tau) \right) \left(n_{d\uparrow}(0) - n_{d\downarrow}(0) \right) \right\rangle \\
&= \int_0^\beta d\tau \, \left\langle \left(1 - \tilde{n}_{d\uparrow}(\tau) - 1 + \tilde{n}_{d\downarrow}(\tau) \right) \left(1 - \tilde{n}_{d\uparrow}(0) - 1 + \tilde{n}_{d\downarrow}(0) \right) \right\rangle \\
&= \int_0^\beta d\tau \, \left\langle \left(\tilde{n}_{d\uparrow}(\tau) - \tilde{n}_{d\downarrow}(\tau) \right) \left(\tilde{n}_{d\uparrow}(0) - \tilde{n}_{d\downarrow}(0) \right) \right\rangle \, .
\end{aligned}
\tag{3.43}
$$

It is invariant! Consequently, we expect it to be symmetric for $\epsilon_d = \pm\Delta\epsilon$ and we can use this fact to check our simulations later on. Conversely, if we're only interested in the spin susceptibility then there's no need to run simulations for both $\epsilon_d = \Delta\epsilon$ and $\epsilon_d = -\Delta\epsilon$, one is sufficient. Finally, it is easily confirmed that just as the spin susceptibility, the potential energy $(n_{d\uparrow} - \frac{1}{2})(n_{d\downarrow} - \frac{1}{2})$ is invariant under a particle-hole transformation, whereas the double occupancy $\langle n_{d\uparrow} n_{d\downarrow} \rangle$ is not.

3.5 FROM THE ANDERSON TO THE S-D MODEL

An alternative approach for the treatment of an impurity in a metallic host is taken by the s-d model, which is sometimes equally referred to as s-d exchange model or Kondo model. The s-d model starts from a simple scattering potential, but additionally assumes that the impurity has a local magnetic moment. The model then introduces a Heisenberg exchange interaction between the spins of the impurity and the bath. Consequently, as the presence of the local moment is an a priori presumption, the s-d model is not a suitable device for the study of local moment formation. That's why we stick with the Anderson model for our simulations. However, the s-d model can very well expose the Kondo effect and it was in fact the s-d model that was used in most early investigations into Kondo physics: Kondo himself used it to third order perturbation theory to uncover the resistance minimum in 1964. Anderson undertook the Poor man's scaling with the s-d model first (1970), as well as Wilson, who employed the model for his numerical renormalization group studies in the early seventies.

The Hamiltonian of the s-d model is

$$
\begin{aligned}
H_{sd} = &\sum_{k\sigma} \epsilon_k c_{k\sigma}^\dagger c_{k\sigma} + \sum_{kk'\sigma} V_{kk'} c_{k\sigma}^\dagger c_{k'\sigma} \\
&+ \sum_{kk'} J_{kk'} \left[S_d^+ c_{k\downarrow}^\dagger c_{k'\uparrow} + S_d^- c_{k\uparrow}^\dagger c_{k'\downarrow} + S_d^z \left(c_{k\uparrow}^\dagger c_{k'\uparrow} - c_{k\downarrow}^\dagger c_{k'\downarrow} \right) \right] .
\end{aligned}
\tag{3.44}
$$

The first two terms describe the bath electrons and their scattering off a simple potential $V_{kk'}$. The third term introduces the spin-dependent interaction with a Heisenberg coupling constant $J_{kk'}$. The spin of the impurity is denoted by $\mathbf{S}_d = (S_d^x, S_d^y, S_d^z)$ and, of course, $S_d^\pm = S_d^x \pm iS_d^y$. In contrast, the spin of the bath is noted down implicitly in the form of the k-space creators and annihilators. In the above form of the s-d model the spin-dependent scattering of the conduction electrons

comes out very nicely: On scattering off the impurity the spin of the conduction electron may be flipped.

In a notion equivalent to the local hybridisation approximation discussed in section 3.1, the k-dependence of the coupling constant $J_{kk'}$ can be dropped. Then the interaction is only between the impurity and the first site of the bath. The spin of the bath can be written $\mathbf{S}_{ij} = \frac{1}{2} \sum_{\sigma\sigma'} c^\dagger_{i\sigma} \boldsymbol{\sigma}_{\sigma\sigma'} c_{j\sigma'}$, with the Pauli vector $\boldsymbol{\sigma}$ and the creator and annihilator now in real space. Hence, the s-d model may be cast to the form

$$H_{sd} = \sum_{k\sigma} \epsilon_k c^\dagger_{k\sigma} c_{k\sigma} + \sum_{kk'\sigma} V_{kk'} c^\dagger_{k\sigma} c_{k'\sigma} + J\, \mathbf{S}_d \mathbf{S}_{00} \,. \tag{3.45}$$

In this formulation, the Heisenberg-like interaction between the two spins is most obvious.

The s-d model is an effective low energy model for the Anderson model within suitable parameter ranges. The ground state of the Anderson model must be the singly occupied impurity so that we have a local moment. For the Hamiltonian (3.20) this means $\epsilon_d + \frac{1}{2}U \gg \epsilon_F$ and $\epsilon_d - \frac{1}{2}U \ll \epsilon_F$, where ϵ_F denotes the Fermi energy. Alternatively, we can take the limit where V is constant, ϵ_d small and $U \to \infty$ as a more intuitive definition for the local moment regime of the Anderson model and therefore for the validity of the s-d model. The mapping from the Anderson model to the s-d model is done by the Schrieffer-Wolff transformation. This transformation treats charge fluctuations to the high-energy states – the empty or doubly occupied impurity – perturbatively, as virtual excitations. We won't carry out the calculation here, the procedure is sketched in [16] and attended to in more detail in [17] and [18]. For us the important outcome of the Schrieffer-Wolff transformation is the relation of the Anderson model parameters V, U and ϵ_d of our Hamiltonian (3.20) to the coupling constant J of the s-d model (3.45).

$$J = V^2 \left(\frac{1}{\epsilon_d + \frac{1}{2}U} + \frac{1}{-\left(\epsilon_d - \frac{1}{2}U\right)} \right) \tag{3.46}$$

Note that the coupling constant is positive in the range where the s-d model is applicable and thus J induces an antiferromagnetic Heisenberg exchange interaction.

Although we do not employ the s-d model directly, the coupling constant J provides an extremely useful guideline for the evaluation of simulation results. We understand J as an energy scale on which the spin-spin interaction is of relevance.

4

NUMERICAL RESULTS: THERMODYNAMICS AND DYNAMICS FOR THE SIAM

After our long and wearisome way through the preceding chapters, having gained an understanding of both the DDQMC algorithm and the single impurity Anderson model, we're now in the exciting position to present and subsequently discuss results distilled from numerical simulations. Our goal is to investigate an Anderson impurity in a bath. We aim for low temperatures so as to expose the Kondo regime. We want to study thermodynamic properties like the spin susceptibility and the double occupancy as well as dynamic properties, most prominently the spectral function.

4.1 DETERMINING THE KONDO TEMPERATURE

The first step towards rewarding simulations is to find a suitable set of parameters that allows us to capture the physics of interest. However, practically, the accessible range of parameters is limited by the scalability of the DDQMC algorithm and finite computational resources. As we saw in chapter 2.3, the perturbation order scales linearly with the interaction parameter U and the inverse temperature β, while the run-time of the method depends on the perturbation order to the cube. This is most unfortunate as it would surely be nice to use a large U. Together with a smallish hybridisation V (and thus a small peak width[1]) it would yield nicely separated upper and lower Hubbard bands and consequently a large and stable local moment regime with respect to variations in ϵ_d. And varying ϵ_d is after all what we're aiming for. Secondly, we definitely need to access low temperatures so that we can securely and reliably capture the low energy physics, that is, Kondo physics. The question only is, how low is low enough? Now the onset of the Kondo regime can be roughly

---

[1] For the non-interacting Anderson model the peak width of the resonant bound state can be calculated to $\Delta = \pi\rho_0 V^2$, with ρ_0 the density of states of a flat band [16]. This relation serves as a guideline for the interacting Anderson model.

characterised by the Kondo temperature T_K. An estimate for this temperature emerges, for example, from Anderson's Poor man's scaling approach [16],

$$T_K \sim e^{-\frac{1}{2J\rho_0}} \tag{4.1}$$

with the coupling constant from the s-d model J and the density of states ρ_0. We choose a flat band $\rho_0 = \frac{1}{W}$ and set the band width $W = 4$. This flat band approximates a genuine one dimensional cosine band with a hopping parameter $t = 1$. Consequently, the band width W as well as all other parameters will be in units of t. For a starting point let us set $\epsilon_d = 0$ whereby the coupling constant (3.46) becomes

$$J = 4\frac{V^2}{U}. \tag{4.2}$$

It is evident that for a small hybridisation V and a large interaction term U the above equation yields a small J and as a result an exponentially small Kondo temperature; which in turn gets increasingly impossible to achieve with DDQMC. Clearly we're in a conflict situation here. We need to find a compromise.

The down-to-earth way of going about this is to run a number of test simulations with different sets of parameters. For each run we determine the Kondo temperature. We adapt parameters and iterate the process until we find a set we're satisfied with. We again choose $\epsilon_d = 0$ as a practical starting point. Now from a perturbation theory treatment of the s-d model we know that the spin susceptibility adheres to a Curie-Weiss law for $T \gg T_K$ [16].

$$\chi^{-1}(T) \sim \mathrm{const} \cdot (T + 4.5 T_K) \tag{4.3}$$

This is promising candidate to extract the Kondo temperature! However, the s-d model (section 3.5) is only valid in the local moment regime. As we will see in the next section, that means an upper bound for the temperature $T < U$ at $\epsilon_d = 0$. Therefore we plot the inverse spin susceptibility over temperature and fit the above Curie-Weiss law in the applicable range, which we practically choose to $\left[10 T_K, \frac{U}{2}\right]$.

Figure 1 demonstrates the procedure for our final set of parameters, $W = 4, U = 2, V = 0.75$ (in units of t), yielding a Kondo temperature $T_K = 0.017$. Appreciate how the data really replicates the Curie-Weiss law in the range from $10 T_K \sim 0.2$ to $\frac{U}{2} \sim 1$ and deviates in the ranges above and below. For $\beta = 120$ corresponding to $T = 0.008$, so well within the Kondo regime for the chosen parameters, we get a perturbation order of $\langle n \rangle = 90$ for $\delta = 0.51$. Remember that δ was originally introduced in chapter
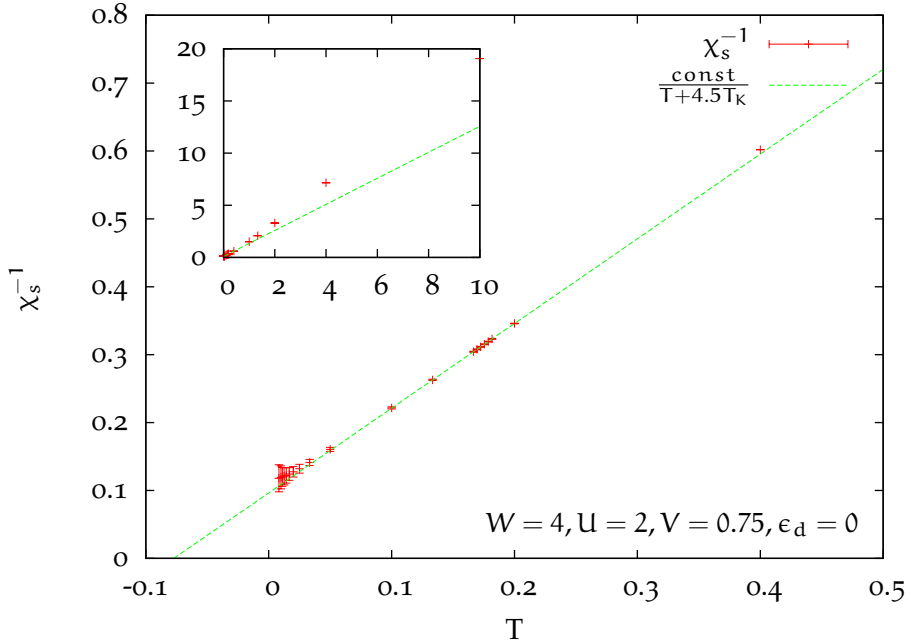
Figure 1: Inverse spin susceptibility over temperature at $\epsilon_d = 0$. The spin susceptibility adheres to a Curie-Weiss law in the range from $10T_K \sim 0.2$ to $U/2 \sim 1$, roughly corresponding to the local moment regime. The Kondo temperature is the zero-crossing point of the fit up to a constant factor.

3.2 to get a grip on the sign problem. For $\epsilon_d = 0$ we can set $\delta = 0.1$ and achieve an average perturbation order as low as $\langle n \rangle = 30$. Well, orders of 30 or 90 are quite feasible. Henceforth we shall employ this set of parameters unless stated otherwise.

4.2 THE ANDERSON IMPURITY AT $\epsilon_d = 0$

For the time being we concentrate on an impurity with $\epsilon_d = 0$. This simpler and more common case displays all scales and properties relevant for the Kondo problem and a thorough understanding will help us set the ground for the impurity deviating from

symmetry, which we consider in the next section. For $\epsilon_d = 0$ the Anderson model is often referred to as the *symmetric* Anderson model. The Hamiltonian (3.20) becomes

$$H = \sum_k \epsilon_k n_k + \frac{V}{\sqrt{N}} \sum_k \left(d^\dagger c_k + c_k^\dagger d \right) + U \left(n_{d\uparrow} - \frac{1}{2} \right) \left(n_{d\downarrow} - \frac{1}{2} \right) , \qquad (4.4)$$

where spins are implicit except for the interaction term. As they were seen to leave the physics invariant, Ising spins need not be included for our discussion.

Figure 2 displays a pictogram of the system under consideration for the parameter set introduced in the preceding section. On the left is the impurity with the upper and lower Hubbard band at the electron energies $\epsilon_d \pm \frac{U}{2} = \pm 1$, separated by the Hubbard interaction parameter $U = 2$. Each level exhibits a broadening $\Delta = \pi \rho_0 V^2 = 0.44$ resulting in a small overlap of the upper and lower band. The impurity is embedded in a bath with a flat band of bandwidth $W = 4$. Although we're employing a flat band we will keep on thinking in the more intuitive picture of a one-dimensional chain of lattice sites with an inter-site hopping of $t = 1$. A one-dimensional chain with nearest-neighbour-hopping exhibits a cosine band structure; the flat band is a reasonably good approximation to the cosine band near the centre of the band. The Fermi energy is $\epsilon_F = 0$, thus the band is half-filled, with a small broadening of the Fermi level due to a finite temperature of (very roughly) $T = 1$. Lastly, we are using the local hybridisation approximation so that the hybridisation between impurity and bath is more accurately thought of as a hopping between the impurity and the first bath site with a hopping parameter V.

Keeping this picture in mind we now turn to the discussion of the double occupancy and the spin susceptibility which we have measured over temperature. Additionally to these thermodynamic quantities we will also have a look at the spectral function at selected temperatures. The spectral function $A(\omega)$ is a dynamic property extracted from the imaginary time resolved Green's function $G(\tau)$ by means of the stochastic maximum entropy method (MaxEnt for short). In contrast to DDQMC this method is not exact in a physical sense and can be problematic. We have employed a flat default model, setting aside prior knowledge. We have not symmetrised input data, nor smoothed output data. Thus the graphs of the dynamic properties presented here are a mirror of both the quality of the DDQMC data and the problems of the maximum entropy method. Despite these deficiencies, the spectral functions obtained provide a very intuitive picture as we can think of them as energy resolved densities of electron states on the impurity. We can quite literally take them and put them in our nice little pictogram 2. Indeed, it can be shown that $A(\omega)$ *is* the density of states induced by
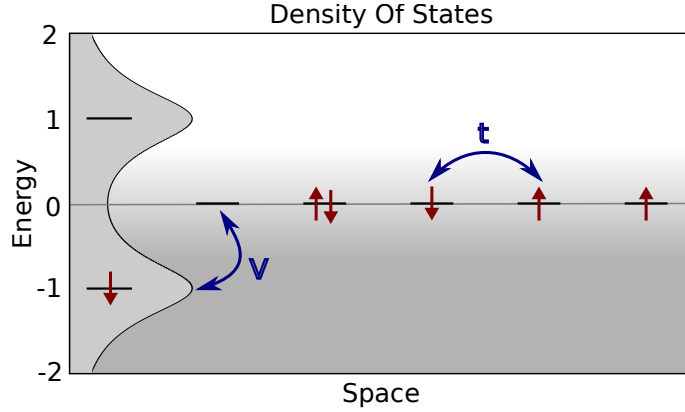
Figure 2: Anderson impurity at $\epsilon_d = 0$. The impurity (left) with the broadened upper and lower Hubbard band at $\epsilon_d \pm \frac{U}{2} = \pm 1$ embedded in a bath (right). The bath is a one-dimensional chain of lattice sites with nearest-neighbour hopping t and bandwidth $W = 4$. Hopping of the electrons from the impurity to the first bath site and back is characterised by the hybridisation V. The depicted situation corresponds to the local moment regime where the lower level is singly occupied while the upper level is thermally vacated. The temperature is roughly $T \sim 1$.

the impurity within the context of the non-interacting Anderson model and near the centre of the band [16].

The double occupancy most beautifully exposes all relevant scales of the Kondo problem. Thus we concentrate on the double occupancy, figure 4, and we start in the high temperature limit. Let $T \to \infty$ and U finite, then both impurity levels are equally occupied. The band is half-filled, the particle number on the impurity therefore $N = 1$ and consequently $n_\uparrow = \frac{1}{2}$ as well as $n_\downarrow = \frac{1}{2}$. The expected double occupancy becomes $\langle n_\uparrow n_\downarrow \rangle = \frac{1}{4}$ in this limit and from the plot we gather $\langle n_\uparrow n_\downarrow \rangle \to 0.24$ as T approaches 10 which confirms the assertion. Indeed, for the temperature much larger than the interaction parameter we can neglect U and consider the problem with the non-interacting Anderson model. Here the impurity becomes a simple (spin-independent) scattering potential with a single virtual bound state resonance at the centre of the band, $\epsilon = \epsilon_d \pm \frac{U}{2} \sim 0$. The spectral function at $T = 4$ impressively verifies this line of thinking, figure 5.

Peaking ahead at the spectral function at $T = 1$ we recognise two clearly discernible Hubbard bands located at $\epsilon = \pm 1$. This situation comes close to the pictogram 2
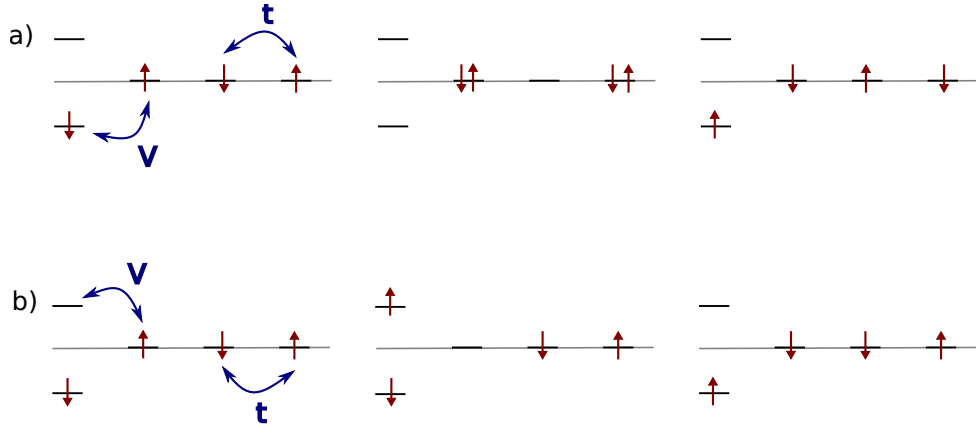
Figure 3: Superexchange processes. a) The impurity is temporarily vacated as the impurity electron "hops" to the bath. b) The impurity is temporarily double occupied as a bath electron "hops" to the impurity. Local hybridisation asserts that there is only hopping between the first bath site and the impurity, characterised by V. The intra-bath-hopping is characterised by the hopping parameter t.

discussed above and it is the local moment regime. We understand the local moment regime thinking in opposite limits as before: $U \to \infty$ and T finite. Now the lower impurity level is singly occupied while the upper is thermally vacated. Accordingly, the double occupancy is zero and, as the interaction parameter is very large, we can consider the hybridisation arbitrary small as well, $V \to 0$. The emerging picture is that of an isolated impurity with a free spin, a local moment. Hence the name of the regime. The spin susceptibility is expected to show a Curie-like behaviour and in fact we have seen a Curie-Weiss law in figure 1 in the preceding section. There we put it to use to extract the Kondo temperature. Conversely, we can make out the adherence to a Curie-Weiss-like behaviour as a definition for the local moment regime. More generally, we will usually employ the singly occupied impurity (commonly denoted as d^1) and a mostly free spin as loose defining characteristics of this regime. Returning to finite parameters we consequently identify the Hubbard interaction U as the upper boundary of the local moment regime for the symmetric Anderson model. The interaction parameter competes with the temperature. Thus, as we decrease the temperature from $T \gg U$ to $T \lesssim U$ we *cross over* from the high temperature regime to the local moment regime. Glancing at the double occupancy graph 4 we again see our assertion fulfilled: Starting at 0.25 for high temperatures it drops towards zero as
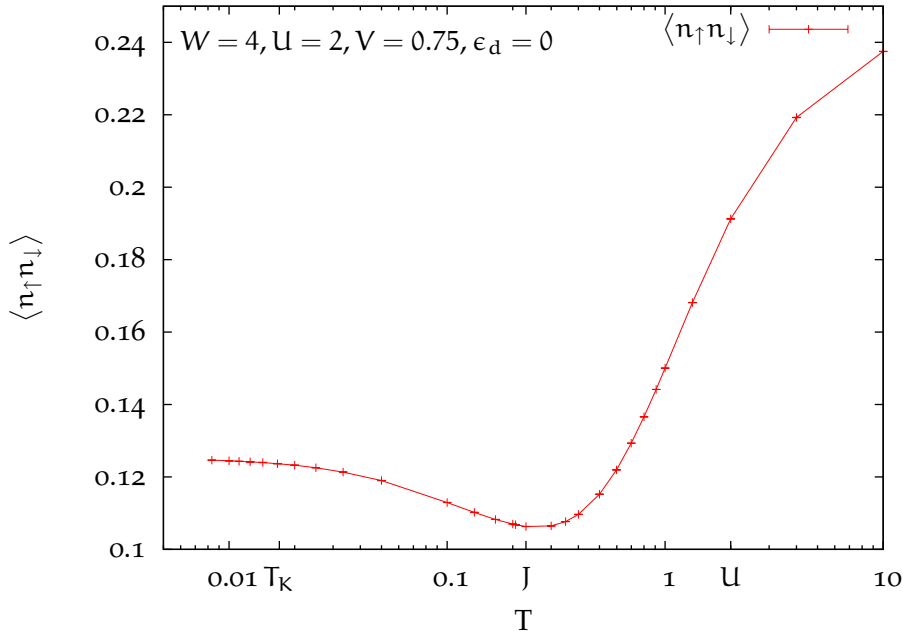
Figure 4: Double occupancy over temperature at $\epsilon_d = 0$. The double occupancy exposes all scales of the Kondo problem: The high temperature regime for $T \gg U$, $\langle n_\uparrow n_\downarrow \rangle \sim 0.25$. The local moment regime for $T < U$, $\langle n_\uparrow n_\downarrow \rangle$ minimal. The Kondo regime for $T \lesssim T_K$, $\langle n_\uparrow n_\downarrow \rangle$ saturates. The Heisenberg coupling constant $J \sim 0.23$ is estimated by the minimum of $\langle n_\uparrow n_\downarrow \rangle$.

we cross below U. However, it recovers before crashing into the baseline, never really getting close to a value of zero and, more astonishing still, even starts to increase again as we further lower the temperature. How can we understand this behaviour?

First note that we would indeed see a $\langle n_\uparrow n_\downarrow \rangle = 0$ region if we took, as before, the large U limit. This would effectively push the high temperature behaviour as well as the drop to the local moment regime to higher temperatures still. The double occupancy would fall to zero in earnest, exposing a very well defined local moment region. Of course, here we have assumed that increasing the interaction parameter would keep the low temperature features of our graph untouched. It should become apparent in a minute that this is not correct. A growing interaction U will push the low temperature features to lower temperatures still which is just as well for our line
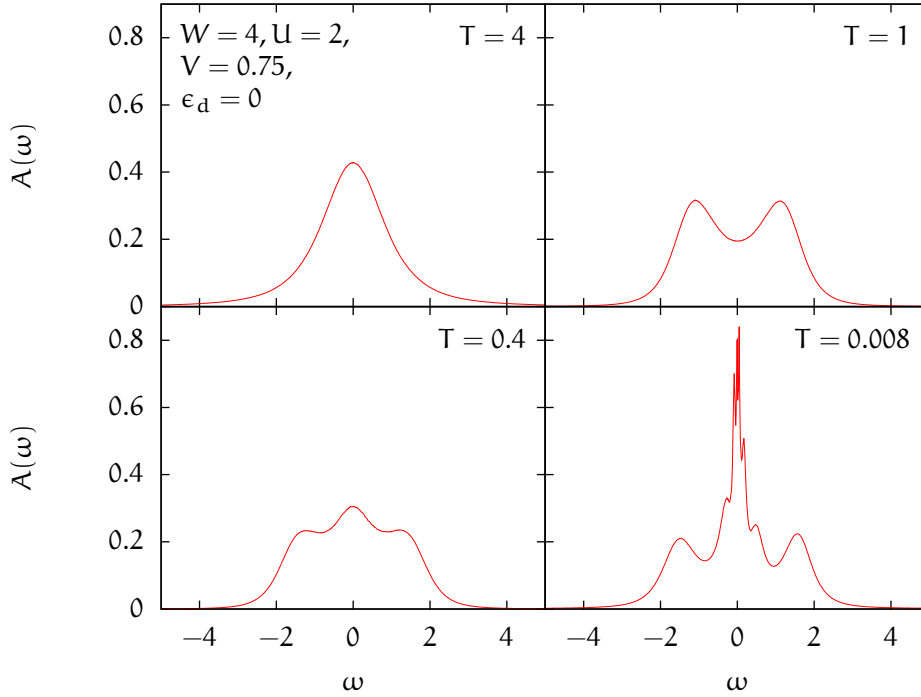
Figure 5: Spectral function at different temperatures. (T = 4) The high temperature regime,
T ≫ U. There is a single virtual bound state resonance at ϵ = 0. (T = 1) The local
moment regime, T < U. The two Hubbard bands are clearly discernible at ϵ = ±1.
(T = 0.4) At the crossover from the local moment regime to the Kondo regime, T < J.
The Kondo resonance becomes visible. (T = 0.008) In the Kondo regime, T ≲ T_K. The
Kondo resonance is now very prominent.

of argumentation. We conclude for the moment that in our measurement the local
moment regime is a bit "cramped". Now it is in the local moment regime that the s-d
model starts to become applicable. The s-d model understands the singly occupied
impurity as a spin which couples to the spin of the bath with an antiferromagnetic
(i.e. positive) Heisenberg coupling constant J. Going from the Anderson model to the
s-d model we appreciate that the superexchange processes of the former – depicted
in figure 3 – and the coupling of spins of the latter really describe the same physical
circumstances. Put another way, the coupling constant J ∼ $\frac{V^2}{U}$ attaches an energy to
the virtual exchange processes; and it makes perfect sense: The "electron hopping" of
the superexchange will appear more frequent for a larger hybridisation V (which we

can interpret as a hopping parameter anyway) and thus lead to larger J. Reversely, the hopping will get increasingly harder for a growing U which pushes the impurity levels further away from the Fermi energy. Consequently, the coupling constant J decreases as the spins are now more weakly coupled, the possible energy gain due to the virtual processes gets smaller.

Although the s-d model definitely evokes the correct qualitative picture in the local moment regime, it is important to keep in mind, that, very strictly speaking, it is only correct in the limits $V \to 0$ for a fixed U or, reversely, $U \to \infty$ for constant V. Hence, for a quantitative assessment we have to be careful with this model. Calculating the coupling constant from the s-d model formula (4.2) yields $J = 1.25$ for our parameters. Looking at graph 4 that does not seem like a very reasonable value. We asserted that J is the energy scale on which the virtual superexchange processes become of importance. Practically, we therefore estimate the Heisenberg coupling constant by the minimum of the double occupancy, $J \sim 0.23$.

In thought starting out from a genuine local moment regime with a zero double occupancy, it is now a competition between temperature and coupling constant (and thus superexchange) that drives the emerging physical picture as we lower temperature once more. For $T \gg J$ the energy gain by virtual exchange processes is largely irrelevant, the impurity spin is thermally disordered, effectively preventing double occupancy which is thus zero. This is the local moment regime discussed infinitely already. As the temperature approaches the coupling constant, $T \sim J$, we do begin to see the superexchange, $\langle n_\uparrow n_\downarrow \rangle$ starts to increase – after all, one of the virtual processes double occupies the impurity. Lowering the temperature further increases the double occupancy still, until it finally saturates as $T \ll J$ and we have crossed into the Kondo regime. Here the temperature and thermal processes are irrelevant. Here the spin of the impurity and of the bath are perfectly coupled, they are entangled and in that sense build a spin singlet state. The Kondo temperature T_K sets a soft boundary – it's a crossover – between the Kondo regime and the higher temperature local moment regime. Again, we can understand the Kondo temperature T_K as the energy attached to the spin singlet. So to break the singlet we need to spend an energy of T_K and, of course, when the temperature exceeds T_K it does break the singlet.

We've used the local hybridisation approximation where we presumed that only the first lattice site is directly involved with the impurity. Speaking of sites, however, is a treacherous business in this context, because we're implicitly thinking in completely localised electron states. Building a proper Wannier state at the first lattice site

requires all k-states of the band, though. But only electrons in a shell of width T_K around the Fermi energy can contribute, as it is the energy T_K that we gain by the superexchange process. Consequently, a Kondo temperature of the order of the bandwidth would be required for an entangled singlet state made up of the impurity and the first lattice site exclusively. Realistically, and in our case, T_K is much smaller. As T_K decreases fewer and fewer k-states are accessible. The entangled bath electron is increasingly delocalised, spread out over multiple adjacent lattice sites. The picture of a screening cloud emerges. It is centred at the impurity and will extend over a range of very roughly $\frac{1}{T_K}$. The cloud screens the impurity spin. So from the outside the impurity looks like a simple spin-independent scattering potential once more. Inside it's rich. To appreciate this let us look at the spectral functions at $T = 0.4$ and $T = 0.008$, figure 5. The Kondo resonance is clearly visible between the two Hubbard bands. It corresponds to a peak in the electron density at the centre of the band, accounting for the virtual processes which involve hopping of electrons near the Fermi energy. The width of the resonance is roughly T_K as, again, only electrons in a shell of width T_K contribute. The Kondo resonance will become more pronounced as we go from J to T_K in temperature. We see this in the two spectral functions where the first is at $T = 0.4$ and therefore at the beginning of the crossover from the local moment regime to the Kondo regime whereas the second is well within the Kondo regime.

Summarising, Kondo physics as discussed here is largely characterisable by three different scales: the Hubbard interaction parameter U, the Heisenberg coupling constant J and the Kondo temperature T_K. These set the soft boundaries for the high temperature regime, the local moment regime and the Kondo regime. Crossovers from one regime to another are driven by a competition between temperature and the respective scale. If we're feeling pedantic we can additionally make the distinction between a "proper" local moment regime with a free spin within the limits set by U and J, and a more "magnetic" local moment regime with an increasingly coupled spin, bordered by J and T_K. It is crucial to note that the scales U and J and T_K are all interrelated and, although not apparent from our measurements, it is one of the fascinating properties of the Kondo problem that the physics involved can be characterised by the Kondo temperature T_K and T_K only. The Kondo temperature is a scaling invariant. Lastly, appreciate how the deceptively simple Hamiltonian of the Anderson model exposes delicate, rich and most beautiful physics. Knowing only about the interaction U, the Anderson Hamiltonian generates the *emergent* scales J and T_K.

4.3   THE ANDERSON IMPURITY AT $\epsilon_d \neq 0$

Finally, we consider an Anderson impurity which deviates from the symmetric case, we consider $\epsilon_d \neq 0$. This impurity is described by the *asymmetric* Anderson model (3.20). We again have measured the double occupancy and spin susceptibility over temperature, this time, of course, for several different impurity levels ϵ_d. For these values of ϵ_d we additionally computed the spectral function at a fixed temperature. Before we rush to the plots, though, let us take a minute and think about what to expect.

For that purpose the isolated impurity as considered previously, with $V \to 0, T \to 0$, but U finite, is a fertile device. Sweeping ϵ_d from $-\infty$ to ∞ reveals five different regimes. At $\epsilon_d = 0$ we're not surprised to find the local moment regime d^1 where the lower Hubbard band is occupied, but the upper is not. Note that for the discussion at hand we understand the local moment regime to include the previously separately discussed Kondo regime. Increasing ϵ_d, thereby shifting both impurity levels towards the upper edge of the band, we will cross through the mixed valence regime where the lower level is vacated consecutively until it is quite empty. We get to the empty orbital regime d^0. While for the isolated impurity under consideration the mixed valence regime is infinitely small – only the precise point where the lower level is at the Fermi energy – for a finite hybridisation V (and thus broadened Hubbard bands) this regime can become quite large. If we shift the impurity levels towards the lower edge of the band, decreasing ϵ_d, we again cross through a mixed valence regime, this time on the way to the charge doublet regime d^2. Here, both Hubbard bands are fully occupied. For the two limits d^0 and d^2, or equivalently $\epsilon_d \to \infty$ and $\epsilon_d \to -\infty$, we expect the double occupancy to be be zero or one, respectively, as well as a vanishing spin susceptibility. That's pretty boring. Of course, in the d^1 regime we're confident to find a Kondo effect if we only take the temperature low enough. The exciting question is, what happens in between? What happens in the upper and lower mixed valence regime and how exactly will the transition look like as we take $|\epsilon_d|$ from zero to infinity?

Now it is in the local moment regime where the s-d model is valid and it is the s-d model that generates the Kondo effect. Sure, the Anderson model exposes the Kondo regime just as well for suitable parameter ranges and this is precisely what we've done in the preceding section. However, the s-d model is a much more stringent requirement, it is a subset of the Anderson model. We can view the validity of the s-d model as a prerequisite for the observation of a Kondo regime – as the s-d

model breaks down, so must the Kondo effect. We shortly discussed the mapping of the Anderson model to the energetic subspace of the s-d model in chapter 3.5. We stated that the mapping is carried out by the Schrieffer-Wolff transformation which considers charge fluctuations from the local moment ground state d^1 to the d^2 and d^0 states as virtual excitations. But as we move towards the mixed valence regime by increasing or decreasing ϵ_d, this assumption breaks down. The charge fluctuations can no longer be treated perturbatively. Still, in the region where the s-d model is applicable – and we can at least in thought extend this range by taking the limit $U \to \infty$ – the Schrieffer-Wolff transformation yields the relation (3.46) which we restate here for convenience.

$$J = V^2 \left(\frac{1}{\frac{1}{2}U + \epsilon_d} + \frac{1}{\frac{1}{2}U - \epsilon_d} \right) \tag{4.5}$$

This formula connects the parameters of the Anderson model to the s-d model and, of course, for $\epsilon_d = 0$ it reduces to the form which we have used extensively in the last section. Apparently, the coupling constant J is symmetric for $\epsilon_d = \pm\Delta\epsilon$ which we understand quite intuitively by considering the hopping processes of the pictogram 3, again. Additionally, we gather from eq. (4.5) that the coupling increases for the asymmetric case.

As before, we're working with a flat band of bandwidth $W = 4$, a Hubbard interaction $U = 2$ and a hybridisation $V = 0.75$, all in units of t. With this parameter set we expect the upper and lower mixed valence regime to be centred around $\epsilon = \frac{U}{2} = 1$ and $\epsilon = -\frac{U}{2} = -1$, respectively. And indeed, when we now turn our attention to the double occupancy which we measured over temperature for ϵ_d ranging from -1.5 to $+1.5$, figure 6, we gather that for $|\epsilon_d| < 1$ there is a Kondo effect, while for $|\epsilon_d| \geqslant 1$ there is none. Here we have used the minimum in $\langle n_\uparrow n_\downarrow \rangle$ and, going to lower temperatures, the adjacent ascending slope as identifying characteristics of the Kondo effect. In the last section we employed the position of the minimum of the double occupancy as the correct value of the Heisenberg coupling constant J, which in practice differs from the value calculated from the s-d model. Nevertheless the s-d model may very well serve as a guideline. Eq. (4.5) yields $J(\epsilon_d = 0) = 1.125$ and $J(\epsilon_d = \pm 0.5) = 1.5$ and from the graph we read off the minima $\min(\epsilon_d = 0) = 0.23$, $\min(\epsilon_d = +0.5) = 0.35$ and $\min(\epsilon_d = -0.5) = 0.30$. So while we fulfil the assertion that the coupling J increases as the impurity deviates from $\epsilon_d = 0$ we can't necessarily confirm that it is symmetric. However, the minimum of the double occupancy is the result of the superposition of the low temperature and high temperature features.
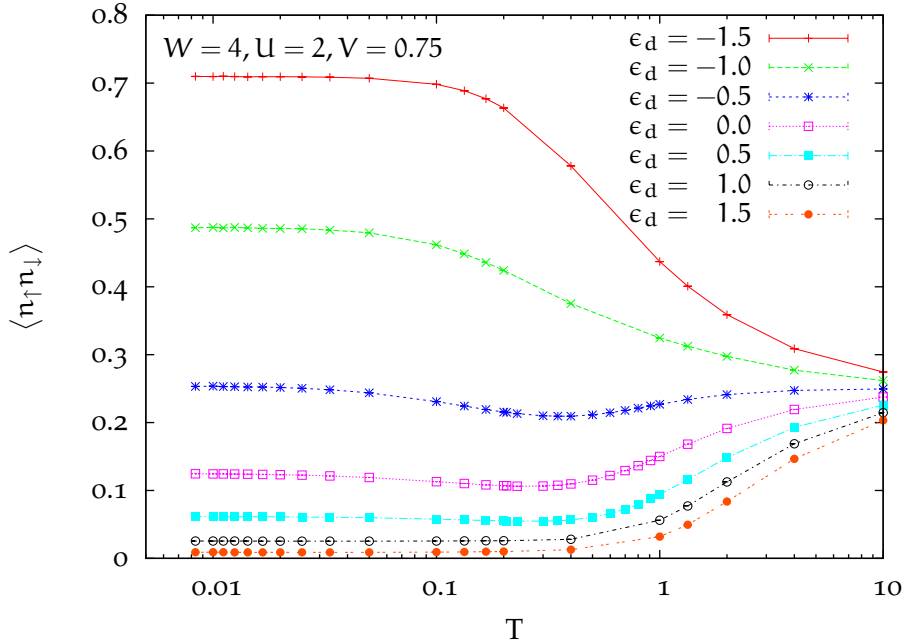
Figure 6: Double occupancy over temperature for different values of ϵ_d. For $\epsilon_d = -0.5, 0.0, 0.5$ the double occupancy exhibits a minimum and adjacent ascent as temperature is lowered. This is the local moment regime d^1 with a Kondo effect at low temperatures. For $|\epsilon_d| = 1.0, 1.5$ the impurity is in the mixed valence regime – at the transition to the charge doublet regime d^2 ($\epsilon_d = -\infty$, $\langle n_\uparrow n_\downarrow \rangle = 1$) and the empty orbital regime d^0 ($\epsilon_d = \infty$, $\langle n_\uparrow n_\downarrow \rangle = 0$), respectively. The local magnetic moment disappears, the Kondo effect breaks down.

While the low temperature features are symmetric just as J from (4.5), the high temperature features are asymmetric with respect to ϵ_d, so we wouldn't expect the minimum to reflect the symmetry of the coupling constant from the s-d model.

Let us now look at the double occupancy for $|\epsilon_d| \geqslant 1$, we start with $|\epsilon_d| = 1$. This is the mixed valence regime par excellence as we have one level of the impurity exactly at the Fermi energy $\epsilon_F = 0$. The curves are understood by thinking in thermal occupation and vacation exclusively. Consider, for example, $\epsilon_d = -1$. The upper Hubbard band is exactly half occupied, while the lower band is completely filled, apart from the tiniest tail extending beyond $\epsilon = 0$. Consequently, we expect the

double occupancy to be just a tad below $\langle n_\uparrow n_\downarrow \rangle \sim 0.5$ and glancing at the graph 6 we see this argumentation impressively verified. Moving the impurity levels further away from the Fermi energy still, $|\epsilon_d| = 1.5$, we notice that the double occupancy saturates at higher temperatures than at $|\epsilon_d| = 1$. This behaviour is again understood by considering the thermal processes at work. The behaviour is the result of the overlap of the thermally broadened Fermi function and the V-broadened Hubbard bands. For higher $|\epsilon_d|$ the Fermi function will overlap with the bulge of the bands only at higher temperatures. For decreasing $V \to 0$ we would expect the transition from the high temperature $\langle n_\uparrow n_\downarrow \rangle \sim 0.25$ to the lower temperature saturation regime to get sharper.
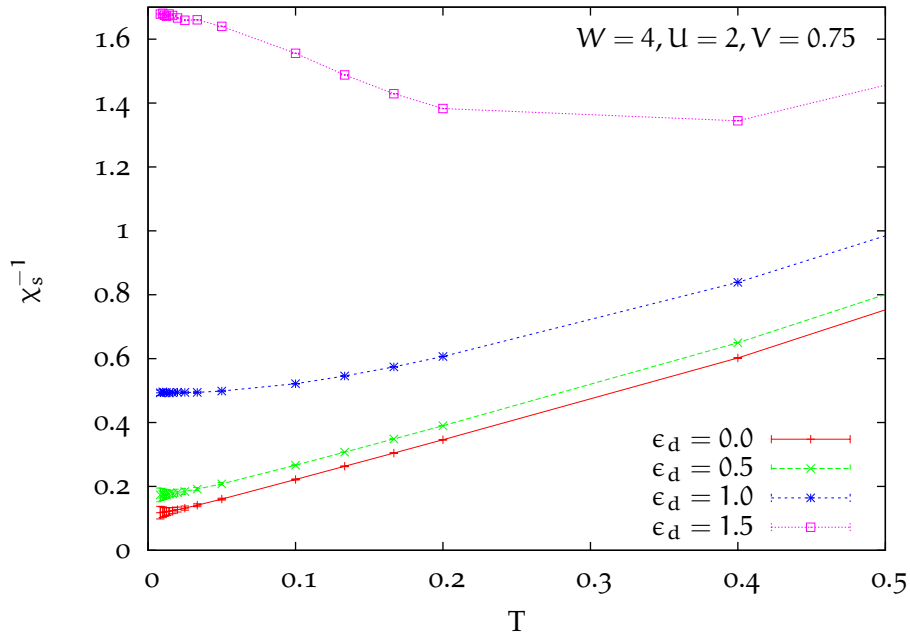
Figure 7: Inverse spin susceptibility over temperature for different values of ϵ_d. For $\epsilon_d = 0.0, 0.5$ the inverse spin susceptibility mostly resembles a straight line, it follows a Curie-Weiss law. This is the local moment regime. At $\epsilon_d = 1.0$ the plot gets curvier. At $\epsilon_d = 1.5$ the impurity has clearly left the local moment regime – it is in the mixed valence regime.

The inverse spin susceptibility, figure 7, mirrors the breakdown of the local moment regime we deduced from the double occupancy plot. In the local moment regime the spin susceptibility is expected to adhere to a Curie-Weiss law. In other words, the inverse spin susceptibility over temperature should be a straight line. Temperature-wise the upper limit of the local moment regime was seen to roughly correspond to $U/2$ for the symmetric case $\epsilon_d = 0$. For ϵ_d deviating from zero, we expect the limit to decrease as now the lower Hubbard band gets vacated, the upper Hubbard band occupied, already at lower temperatures. The plot shows the range from $T = 0$ to $T = 0.5$ where we expect a very clean Curie-Weiss behaviour at least for $\epsilon_d = 0$. Qualitatively, there's hardly a difference in the spin susceptibility for the curves at $\epsilon_d = 0$ and $\epsilon_d = 0.5$. Both are well-fitted by a straight line in the applicable range, $[10T_K, U/2]$. For $\epsilon_d = 1.0$ the graph gets curvier. At $\epsilon_d = 1.5$ the curve has changed behaviour completely, not with the most imaginative mind of the world does it resemble a Curie-Weiss law. We have left the local moment regime.

Notice how we plotted the inverse spin susceptibility for positive ϵ_d only. The reason is, as we asserted in chapter 3.4, that the spin susceptibility is symmetric for positive and negative ϵ_d of the same modulus. Figure 8 demonstrates this symmetry. Here we measured the susceptibility at $T = 0.008$ over ϵ_d from -2 to 2, so over the whole bandwidth. At this temperature we're well within the Kondo regime for $\epsilon_d = 0$ and expectedly the susceptibility is finite. In the other limit, at $\epsilon = \pm 2$, the band edge, χ_s is seen to drop towards zero. Apparently, at the band edge we're getting close to the d^2 and d^0 regimes. The other important property of the graph is the absence of features as we go from $\epsilon_d = 0$ to $\epsilon_d = \pm 2$. We conclude that the transition from the local moment regime to the mixed valence regime to the empty orbital or charge doublet regime is a crossover.

Just as the spin susceptibility the potential energy $\langle (n_\uparrow - \frac{1}{2})(n_\downarrow - \frac{1}{2}) \rangle$ is expected to be symmetric with respect to ϵ_d. We quickly checked this statement in figure 9. Within the error bars the curves for the same value of $|\epsilon_d|$ match perfectly.

To gain further insight into the crossover from the local moment regime to the charge doublet or empty orbital regime, it is rewarding to study the spectral function. Figure 10 shows our measurements, at $T = 0.008$ and for ϵ_d in the range from -1.5 to 1.5. Let us repeat again that the data presented in the graph is raw: We fed the output of the DDQMC method directly (and unsymmetrised, for $\epsilon_d = 0$) to the stochastic maximum entropy algorithm whose results we did not smooth. Particularly at $\epsilon_d = 0$ the difficulties in resolving the delicate features of the Kondo resonance are obvious. Instead of the expected and physical singular peak we have many very narrow spikes.
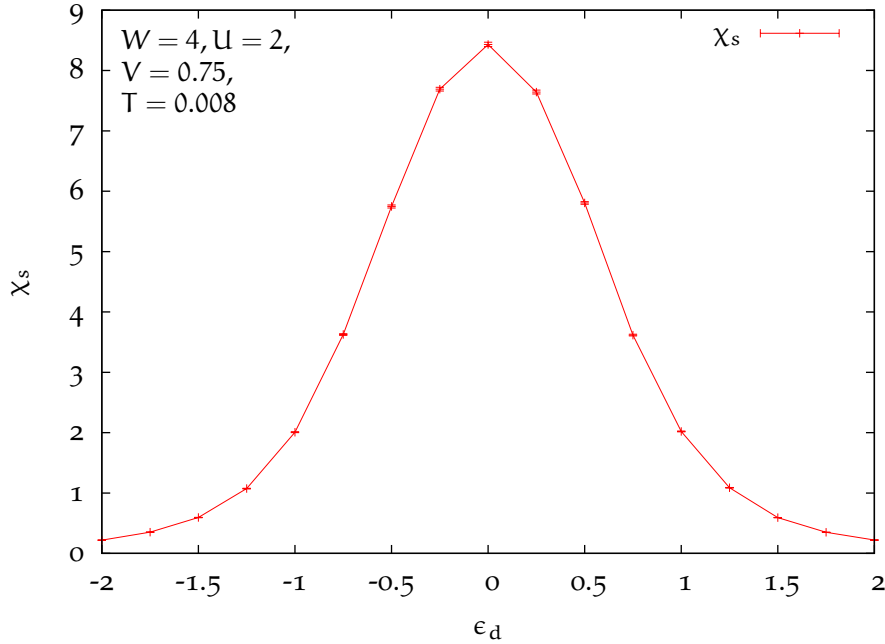
Figure 8: Spin susceptibility over ϵ_d at $T = 0.008$. The spin susceptibility is invariant under a particle-hole transformation and therefore symmetric with regard to ϵ_d. For $T = 0.008$ and $\epsilon_d = 0$ the system is in the Kondo regime. The spin susceptibility is finite. The susceptibility drops off towards zero as $|\epsilon_d| \to \infty$. At $\epsilon_d = \pm 2$, the band edge, the impurity is in the mixed-valence regime, though, arguably, pretty close to d^0 and d^2, respectively, where the susceptibility vanishes.

The symmetric case, $\epsilon_d = 0$, also provides us with an indication of the quality of the MaxEnt data. Knowing that the curve must be symmetric, we can interpret features that deviate from symmetry, for example the smallish bumps at $\epsilon_d \sim \pm 0.5$ in figure 10, $\epsilon_d = 0.0$, as an estimate of the size of the errorbars. We get an understanding to what extend we can trust the MaxEnt results. Consequently, we conclude that these same bumps at $\epsilon_d \sim \pm 0.5$ and similar sized features are safely ignored.
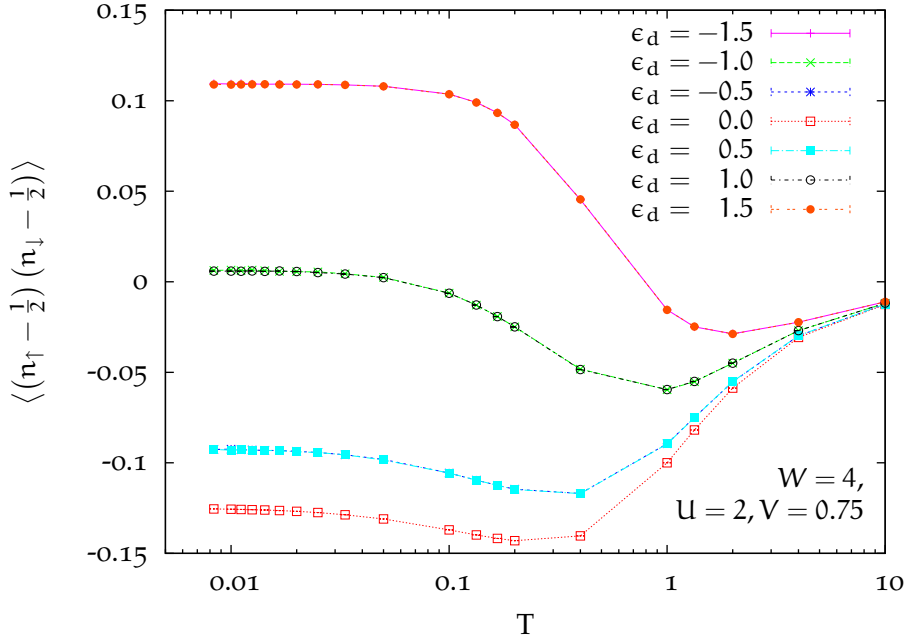
Figure 9: Potential energy over temperature for different values of ϵ_d. The potential energy is invariant under a particle-hole transformation. Consequently, ϵ_d-values with the same modulus yield identical graphs.

This time around, let us attend to the structure of the spectral function $A(\omega)$ in more detail. We consider its symmetry with respect to ϵ_d first. The Lehmann representation of the spectral function is

$$A(\omega) = \sum_{mn} \frac{1}{Z} e^{-\beta \epsilon_n} \left(e^{\beta \omega} + 1 \right) \langle m| \, d \, |n\rangle \, \langle n| \, d^\dagger \, |m\rangle \, \delta \left(\omega - (\epsilon_n - \epsilon_m) \right) . \qquad (4.6)$$

For $\omega > 0$ the spectral function corresponds to the spectrum of the inverse photoemission process (IPES) where an incident electron excites the system which in turn emits a photon. Reversely, the spectrum of the photoemission process (PES) is represented by $A(\omega)$ for $\omega < 0$. Here, of course, incident light results in the system emitting an electron. Intuitively, we might anticipate PES and IPES being connected by a particle-hole transformation, as introduced in chapter 3.4. Indeed, this is readily verified by applying the transformation $d^\dagger \rightarrow -\tilde{d}$, $d \rightarrow -\tilde{d}^\dagger$ to the Lehmann representation

above. We get $A(\omega) \to A(-\omega)$. The particle-hole transformation swaps the PES and IPES part of the spectral function. In chapter 3.4 we also saw that the transformation leaves the Hamiltonian invariant if we only take $\epsilon_d \to -\epsilon_d$. Overall we expect to find $A(\omega) \to A(-\omega)$ for $\epsilon_d \to -\epsilon_d$. But that is just what we observe in our plots, for $\epsilon_d = \pm 1.5$, $\epsilon_d = \pm 1.0$ and $\epsilon_d = \pm 0.5$, respectively!

To understand the position of the peaks of the spectral function we consider the limit $V \to 0$, the isolated impurity, a last time. As the bath is completely decoupled, the Hamiltonian becomes

$$
\begin{aligned}
H_{\text{impurity}} &= \epsilon_d \left(n_{d\uparrow} + n_{d\downarrow} \right) + U \left(n_{d\uparrow} - \frac{1}{2} \right) \left(n_{d\downarrow} - \frac{1}{2} \right) \\
&= \left(n_{d\uparrow} + n_{d\downarrow} \right) \left(\epsilon_d - \frac{1}{2} U \right) + n_{d\uparrow} n_{d\downarrow} U + \frac{U}{4} .
\end{aligned}
\tag{4.7}
$$

Apart from a constant this yields the energy levels $2\epsilon_d$, $\epsilon_d - \frac{1}{2}U$ and 0 for the doubly occupied impurity d^2, the singly occupied impurity d^1 and the vacant impurity d^0, respectively. As a result, we expect to see contributions to the spectral function at the differences of these energy levels, $\epsilon_d \pm \frac{1}{2}U$. Of course, this is just the energy of the electrons on the impurity and for $\epsilon_d = 0$, the d^1 regime, we recover exactly the two Hubbard bands that we discussed at length in section 4.2. Here, for the singly occupied impurity, photoemission processes ($d^1 \to d^0$) as well as inverse photoemission processes ($d^1 \to d^2$) are possible, generating two bumps in the spectral function at $\epsilon = -1$ and $\epsilon = 1$, respectively. For comparison, from our graph with a finite hybridisation V, figure 10, we read off the peak positions at $\epsilon \sim -1.5$ and $\epsilon \sim 1.6$. Returning to the isolated impurity, $\epsilon_d = -1.5$ is a proper d^2 state. The impurity is already doubly occupied, allowing only for the creation of a hole, $d^2 \to d^1$. This is a photoemission process and we get a single peak at $\epsilon = -0.5$. Again, from the plot at finite V we gather $\epsilon \sim -0.8$. Lastly, $\epsilon_d = 1.5$ corresponds to the empty orbital regime, d^0. In contrast to the charge doublet regime only the inverse photoemission process is possible, $d^0 \to d^1$, and $\epsilon = 0.5$, while from the graph we read off $\epsilon \sim 0.8$. All in all we conclude from this short exercise in calculus that the isolated impurity gives the right idea of the structure of the spectral function in the limits d^2, d^0 and d^1, with the exception, of course, of the Kondo resonance.

Taking V finite again, the Hubbard bands are broadened and the Kondo peak emerges. The graph demonstrates this for $\epsilon_d = 0$ and $\epsilon_d = \pm 0.5$ where we most beautifully have the characteristic imprint of the Kondo effect, the three-peak structure with the Kondo resonance at $\epsilon = 0$ and the Hubbard bands to both sides. As observed

already earlier, for these values of ϵ_d we are clearly in the local moment regime. Notice how the Hubbard bands are moving from smaller frequencies to higher frequencies as we sweep ϵ_d from -0.5 to 0.5 whereas the Kondo resonance stays put at $\epsilon = 0$. This is pretty much what we expected, coming from the isolated impurity picture with the energy levels given by $\epsilon_d \pm \frac{1}{2}U$. While this picture and formula are no longer valid they nevertheless serve as a good guideline. The Kondo resonance is a consequence of the hopping of the band electrons to the impurity and therefore it is bound to be centred at the Fermi energy. Not surprisingly, at $\epsilon_d = \pm 1.5$ which we already identified as the d^0 and d^2 regimes, the Kondo resonance has disappeared. Again, the intriguing and tricky question is, what happens in the mixed valence regime, $\epsilon_d = \pm 1.0$. Qualitatively, $\epsilon_d = -1.0$, for example, is much closer to the charge doublet regime d^2 than to the local moment regime d^1: It's a single-peak structure, neither the Kondo resonance nor the Hubbard bands are discernible. We might be tempted to argue that this one peak is a superposition of a decreased Kondo peak and the Hubbard bands, where the left band is diminished while the other is enhanced. However, it is easier and safer to state that the peak is no longer centred at $\epsilon = 0$. This, more than anything else, is a clear indication that the Kondo resonance cannot be a major contribution to the structure of the peak. No longer is the Kondo resonance an important ingredient to the structure of the spectral function. Thus we confirm our earlier assertion that at $\epsilon_d = \pm 1.0$ we've left the local moment regime for good. The s-d model is not valid, the Kondo effect is not observed.

In the last section we investigated the Anderson model at $\epsilon_d = 0$ and for different temperatures. Before the Kondo effect could pronounce itself, a local moment was seen to arise. Similarly, for measurements over various values of ϵ_d as we have carried them out in this section, the local moment would again be present when a Kondo resonance became prominent. We understand the local moment as a prerequisite for Kondo physics to become apparent. We see the formation of a moment most easily by investigation of the inverse spin susceptibility and its adherence to a Curie-Weiss law. Coming from the spin susceptibility we had no problem to identify $\epsilon_d = -0.5, 0.0, 0.5$ as the local moment regime d^1. As the temperature was low enough the imprints of the Kondo effect could be observed in the double occupancy and even more clearly in the spectral function. For $\epsilon_d = \pm 1.0$ the situation was not so clear. It is the mixed-valence regime, a slow crossover from the exciting local moment regime to the more boring regimes where the impurity is either empty or doubly occupied, d^0 and d^2, respectively. Expectedly, the spin susceptibility was seen to vanish, the double occupancy would approach 0 or 1. Although, strictly speaking, for $\epsilon_d = \pm 1.5$

the impurity is still in the mixed-valence regime, we asserted by investigation of the spectral function that qualitatively these values already correspond to the empty orbital and charge doublet regime. The spin susceptibility could not answer the question whether Kondo physics still played a role in the mixed-valence regime at $\epsilon_d = \pm 1$. By virtue of the measurements of the double occupancy, but even more so by the careful evaluation of the spectral function, we were able to assert that at these values of ϵ_d we had clearly departed the Kondo regime and lost the Kondo effect. Our investigations have confirmed impressively that Kondo physics is tightly bound to the presence of a local moment. We loose the local moment by charge fluctuations on the impurity; either driven by a rising temperature or by straight-forward occupation (or vacation) of the impurity as ϵ_d is varied. The phase space of the spin physics is diminished. And as we loose the local moment, so we loose the Kondo physics.
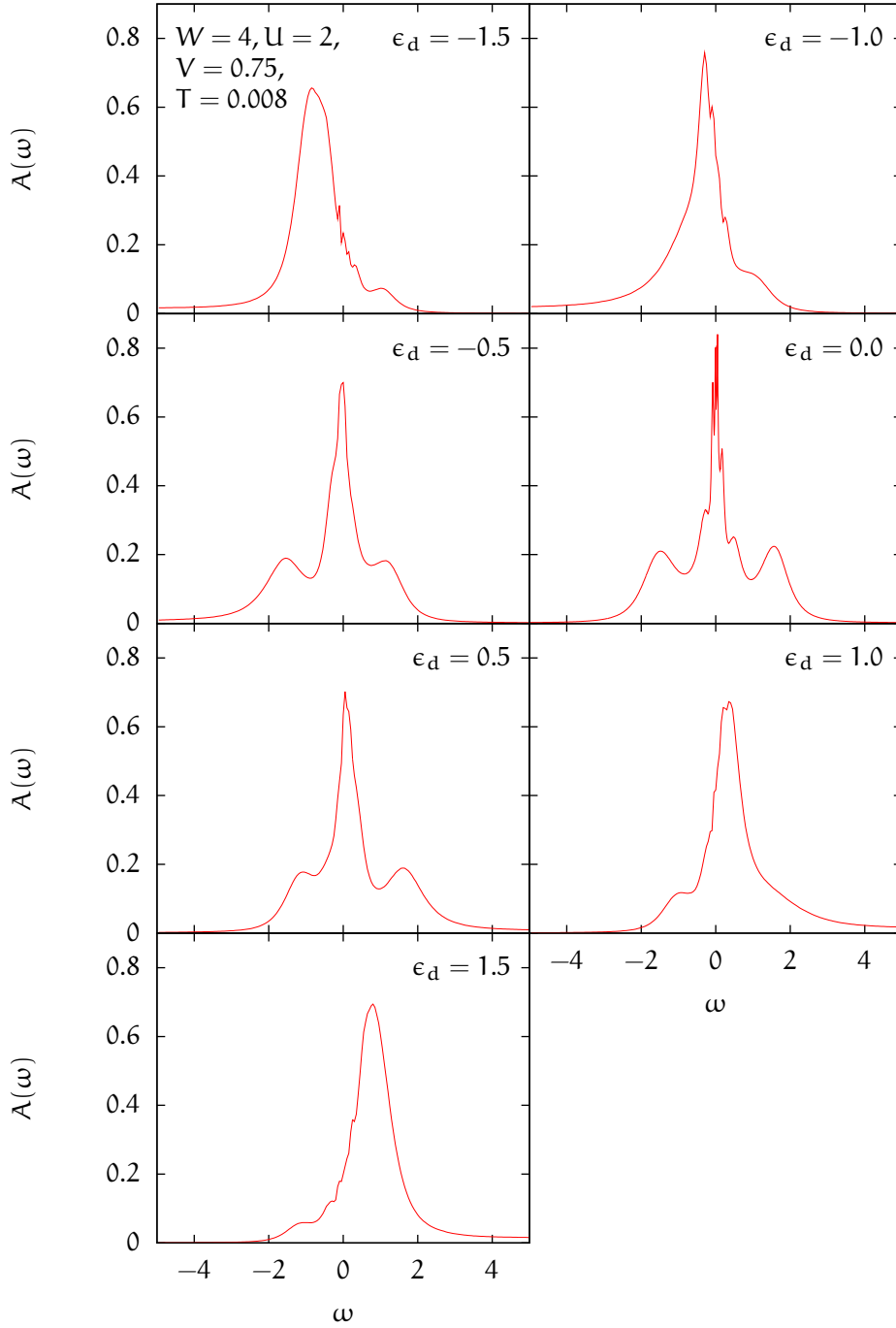
Figure 10: Spectral function at $T = 0.008$ for different values of ϵ_d. ($\epsilon_d = -1.5$) Charge doublet regime, d^2. ($\epsilon_d = -1.0$) Lower mixed-valence regime. ($\epsilon_d = -0.5, 0.0, 0.5$) Local moment regime, d^1, and Kondo regime. The Kondo resonance is prominent between the two Hubbard bands. ($\epsilon_d = 1.0$) Upper mixed-valence regime. ($\epsilon_d = 1.5$) Empty orbital regime, d^0. The spectral function is symmetric with respect to ϵ_d.

5

CONCLUSION

We have implemented the recently developed DDQMC method in a modern, efficient and well-tested C++ program. The code, being written from scratch, was applied to the single impurity Anderson model. Having systematically deduced a parameter set suited to the study of local moment formation and Kondo physics, high quality simulations were then carried out. For the very low temperature ranges a simple parallelisation scheme was devised and successfully put to use, producing very clean and accurate results. From the Green's function the spectral function could be extracted by the Maximum Entropy method. While the spectral function provides a very intuitive and intimate access to the physics, the obtained graphs also demonstrate the difficulties of the unbiased Maximum Entropy method in some parameter ranges, notably at low temperatures. Evaluating the double occupancy, the spin susceptibility and the spectral function measured over temperature, the local moment formation and, at lowest temperatures, the emergence of the Kondo effect were observed and discussed in detail.

Starting from the high temperature limit where the impurity is essentially a simple scattering potential to the conduction electrons, lowering the temperature would lead to a drop in the double occupancy and the development of the two Hubbard bands in the spectral function. This is the local moment regime. We identified the temperature of the crossover into the regime. We saw the formation of the local moment to be related to the Hubbard interaction parameter, for a fixed hybridisation. In the local moment regime, the Curie-Weiss law for the susceptibility could be verified. The emergence of the Kondo effect was observed as the temperature was lowered still. Most notably, the spectral function showed the characteristic three-peak imprint of the Kondo effect, with the developing Kondo resonance at the Fermi energy.

The formation of a local moment on the impurity was studied for a varied ϵ_d, as well. The energy levels of the impurity were shifted from the lower to the upper band edge of the conduction electrons. Carrying out the measurements at very low temperatures, the local moment regime and equally the Kondo effect were observed for the Hubbard bands of the impurity enclosing the Fermi energy. As ϵ_d was pushed

towards the upper or lower band edge, the impurity crossed over to the vacated or doubly occupied regime and the local moment and Kondo physics were lost.

For future work a very exciting prospect lies in the implementation and subsequent observation of the space resolved spin correlations. As the Kondo resonance emerges, this correlation function should reveal the extent and finer structure of the Kondo screening cloud. Heuristically, we have argued to expect the cloud to scale as $\frac{1}{T_K}$ in spatial dimensions. Furthermore we anticipate mid- to long-ranged oscillations in the bath spins, imposed by the screening at the impurity site.

We have extracted an estimate for the Kondo temperature from the Curie-Weiss-like behaviour of the spin susceptibility. This approximative description of the susceptibility emerges from a perturbative treatment of the s-d model that takes the Kondo temperature as the temperature at which the perturbation theory diverges. A more concise definition understands the Kondo temperature as a scaling invariant. Therefore it must be a most rewarding exercise to simulate the problem for different sets of parameters, do a data collapse and observe the fascinating scaling invariance of the whole Kondo problem. As a nice side-effect we would be able to extract the genuine Kondo temperature.

A

TECHNICAL DETAILS OF FAST UPDATES

Update moves in continuous-time quantum Monte Carlo simulations involve calculating the ratio of determinants of the old and the new configuration matrices. For the two most prominent moves, the addition and removal of vertices, the new matrix can be obtained from the old matrix by either adding or removing rows and columns, enabling us to find easy relations for the ratio of determinants. Moreover, the measurement of observables can be thought of as a similar ratio of determinants, again involving matrices related to each other through the addition of rows and columns. It turns out that for these calculations and hence for the simulation at large the knowledge of the inverse configuration matrix is sufficient and luckily, we again can find some relations which allow us to obtain the inverse matrices in a fast way for each update move.

Let us state our results first – an expression for the ratio of determinants and the inverse configuration matrix for the vertex removal and addition move, respectively. To this end we introduce

$$M = \begin{pmatrix} A & B \\ C & D \end{pmatrix}, \qquad M^{-1} = \begin{pmatrix} P & Q \\ R & T \end{pmatrix}, \tag{A.1}$$

$(n+k) \times (n+k)$ matrices, with A and P $n \times n$ matrices and B, C, D as well as Q, R and T sized accordingly. M might be obtained from A in a vertex addition move by adding multiple rows and columns. Reversely, A might be the result of a vertex removal move which started with M. The Schur complement of the block A of matrix M is

$$S = D - CA^{-1}B. \tag{A.2}$$

With these definitions, the following statements hold:

$$\frac{\det A}{\det M} = \det T \tag{A.3}$$

$$A^{-1} = P - QT^{-1}R \tag{A.4}$$

$$\frac{\det M}{\det A} = \det S \tag{A.5}$$

$$M^{-1} = \begin{pmatrix} A^{-1} + B'S^{-1}C' & -B'S^{-1} \\ S^{-1}C' & S^{-1} \end{pmatrix} \tag{A.6}$$

where we used the shorthand notation $B' = A^{-1}B$ and $C' = CA^{-1}$. Appreciate that for vertex removal the knowledge of M^{-1} is all we need; for vertex addition A^{-1} and, of course, the added rows and columns B, C, D are sufficient.

A.1   SETTING FORTH

In our undertaking to derive the above formulas we first state two matrix identities which we will put to use in due course. The *Woodbury identity* is

$$(A + UKV)^{-1} = A^{-1} - A^{-1}U(K^{-1} + VA^{-1}U)^{-1}VA^{-1}, \tag{A.7}$$

where A is a $n \times n$ and K is a $k \times k$ regular matrix. U and V are $n \times k$ and $k \times n$ matrices, respectively. To prove this relation we directly calculate

$$\begin{aligned}
&(A + UKV)(A + UKV)^{-1} \\
&= (A + UKV)(A^{-1} - A^{-1}U(K^{-1} + VA^{-1}U)^{-1}VA^{-1}) \\
&= 1 + UKVA^{-1} - U(K^{-1} + VA^{-1}U)^{-1}VA^{-1} \\
&\quad - UKVA^{-1}U(K^{-1} + VA^{-1}U)^{-1}VA^{-1} \\
&= 1 + UKVA^{-1} - U(1 + KVA^{-1}U)(K^{-1} + VA^{-1}U)^{-1}VA^{-1} \\
&= 1.
\end{aligned} \tag{A.8}$$

Similarly $(A + UKV)^{-1}(A + UKV) = 1$.

For the matrices A, K, U and V a *determinant identity* holds as well:

$$\det(1 + A^{-1}UKV) = \det(1 + KVA^{-1}U) \tag{A.9}$$

Let us show that this statement is valid by using the known relation $\ln \det F = \text{Tr} \ln F$, the series expansion $\ln(1 + F) = \sum_{k=1}^{\infty} \frac{(-1)^{k+1}}{k} F^k$ and the cyclic property of the trace.

$$
\begin{aligned}
\det(1 + A^{-1}UKV) &= \exp\left[\text{Tr}\ln(1 + A^{-1}UKV)\right] \\
&= \exp\left[\sum_{k=1}^{\infty} \frac{(-1)^{k+1}}{k} \text{Tr}\left(A^{-1}U(KVA^{-1}U)^{k-1}KV\right)\right] \\
&= \exp\left[\text{Tr}\ln(1 + KVA^{-1}U)\right] \\
&= \det(1 + KVA^{-1}U)
\end{aligned}
\tag{A.10}
$$

Note that in the following $K = K^{-1} = 1$ will simplify the two stated identities.

A.2 VERTEX ADDITION

We write our new configuration matrix M as

$$
\begin{aligned}
M &= \begin{pmatrix} A & B \\ C & D \end{pmatrix} = \begin{pmatrix} A & 0 \\ 0 & 1 \end{pmatrix} + \begin{pmatrix} B \\ 0 \end{pmatrix}\begin{pmatrix} 0 & 1 \end{pmatrix} + \begin{pmatrix} 0 \\ 1 \end{pmatrix}\begin{pmatrix} C & D-1 \end{pmatrix} \\
&= A_{ex} + U_1 V_1 + U_2 V_2 \, .
\end{aligned}
\tag{A.11}
$$

We evaluate $\det M$ by applying the determinant identity two times. To simplify the calculation we first introduce $\tilde{M} = A_{ex} + U_1 V_1$ and compute its inverse using the Woodbury identity:

$$
\begin{aligned}
\tilde{M}^{-1} &= (A_{ex} + U_1 V_1)^{-1} \\
&= A_{ex}^{-1} - A_{ex}^{-1} U_1 (1 + \underbrace{V_1 A_{ex}^{-1} U_1}_{0})^{-1} V_1 A_{ex}^{-1} \\
&= A_{ex}^{-1}(1 - U_1 V_1 A_{ex}^{-1}) = A_{ex}^{-1}(1 - U_1 V_1) \\
&= \begin{pmatrix} A^{-1} & -A^{-1}B \\ 0 & 1 \end{pmatrix}
\end{aligned}
\tag{A.12}
$$

Now the determinant is

$$
\begin{aligned}
\det M &= \det(\tilde{M} + U_2 V_2) \\
&= \det \tilde{M} \det(1 + \tilde{M}^{-1} U_2 V_2) \\
&= \det A_{ex} \det(1 + V_1 A_{ex}^{-1} U_1) \det(1 + V_2 \tilde{M}^{-1} U_2) \\
&= \det A \det \left[1 + \begin{pmatrix} C & D-1 \end{pmatrix} \begin{pmatrix} A^{-1} & -A^{-1}B \\ 0 & 1 \end{pmatrix} \begin{pmatrix} 0 \\ 1 \end{pmatrix} \right] \\
&= \det A \det(D - CA^{-1}B) = \det A \det S,
\end{aligned}
\tag{A.13}
$$

yielding

$$
\frac{\det M}{\det A} = \det S,
\tag{A.14}
$$

but this is precisely result (A.5).

We obtain the inverse matrix M^{-1} as given by (A.6) by applying the Woodbury identity a second time:

$$
\begin{aligned}
M^{-1} &= (\tilde{M} + U_2 V_2)^{-1} \\
&= \tilde{M}^{-1} - \tilde{M}^{-1} U_2 (1 + V_2 \tilde{M}^{-1} U_2)^{-1} V_2 \tilde{M}^{-1} \\
&= \begin{pmatrix} A^{-1} & -A^{-1}B \\ 0 & 1 \end{pmatrix} \\
&\quad - \begin{pmatrix} A^{-1} & -A^{-1}B \\ 0 & 1 \end{pmatrix} \begin{pmatrix} 0 \\ 1 \end{pmatrix} S^{-1} \begin{pmatrix} C & D-1 \end{pmatrix} \begin{pmatrix} A^{-1} & -A^{-1}B \\ 0 & 1 \end{pmatrix} \\
&= \begin{pmatrix} A^{-1} & -A^{-1}B \\ 0 & 1 \end{pmatrix} - \begin{pmatrix} -A^{-1}B \\ 1 \end{pmatrix} S^{-1} \begin{pmatrix} CA^{-1} & S-1 \end{pmatrix} \\
&= \begin{pmatrix} A^{-1} & -B' \\ 0 & 1 \end{pmatrix} - \begin{pmatrix} -B'S^{-1}C' & -B' + B'S^{-1} \\ S^{-1}C' & 1 - S^{-1} \end{pmatrix} \\
&= \begin{pmatrix} A^{-1} & 0 \\ 0 & 0 \end{pmatrix} + \begin{pmatrix} B'S^{-1}C' & -B'S^{-1} \\ S^{-1}C' & S^{-1} \end{pmatrix}
\end{aligned}
\tag{A.15}
$$

A.3   VERTEX REMOVAL

We establish a multitude of relations between the matrix elements by noting that, of course, $MM^{-1} = M^{-1}M = 1$.

$$M^{-1}M = \begin{pmatrix} P & Q \\ R & T \end{pmatrix} \begin{pmatrix} A & B \\ C & D \end{pmatrix} = \begin{pmatrix} PA + QC & PB + QD \\ RA + TC & RB + TD \end{pmatrix} = \begin{pmatrix} 1 & 0 \\ 0 & 1 \end{pmatrix} \tag{A.16}$$

$$MM^{-1} = \begin{pmatrix} A & B \\ C & D \end{pmatrix} \begin{pmatrix} P & Q \\ R & T \end{pmatrix} = \begin{pmatrix} AP + BR & AQ + BT \\ CP + DR & CQ + DT \end{pmatrix} = \begin{pmatrix} 1 & 0 \\ 0 & 1 \end{pmatrix} \tag{A.17}$$

Using these equations it's easy to show that indeed

$$A^{-1} = P - QT^{-1}R \tag{A.18}$$

as stated in (A.4). We simply calculate $A^{-1}A$:

$$\begin{aligned} A^{-1}A &= PA - QT^{-1}RA \\ &= 1 - QC + QT^{-1}TC \\ &= 1 \end{aligned} \tag{A.19}$$

Similarly, let us apply the above expression for A^{-1} and the relations (A.16) and (A.17) to the Schur complement S.

$$\begin{aligned} S &= D - CA^{-1}B \\ &= D - CPB + CQT^{-1}RB \\ &= D + DRB + (1 - DT)T^{-1}(1 - TD) \\ &= D + D(1 - TD) + (1 - DT)T^{-1}(1 - TD) \\ &= T^{-1} \end{aligned} \tag{A.20}$$

Together with (A.5) this leads to

$$\frac{\det A}{\det M} = \det S^{-1} = \det T. \tag{A.21}$$

Finally we note that should we desire to remove a vertex which is not the last vertex, we can swap rows and columns to obtain the required form of M – so that the rows and columns which are to be removed are the last – do the calculation of A^{-1} and

swap the rows and columns right back in A^{-1}. This works as swapping a row in a matrix corresponds to swapping the same column in its inverse matrix and vice versa. We can even omit the final swapping in A^{-1} if we only keep track of the order of the vertices as we swap rows and columns in M – after all, the order of the vertices doesn't matter in principle.

B

RESOLVENT GREEN'S FUNCTION

Given a general one-particle Hamiltonian with the fermionic creation and annihilation operators $c_i^\dagger$ and c_j,

$$H = \sum_{i,j} \langle i| H |j \rangle \, c_i^\dagger c_j = \sum_{i,j} T_{i,j} c_i^\dagger c_j \,, \tag{B.1}$$

we can find a formal solution for the Green's function

$$G_{i,j}(\tau) = - \left\langle \mathcal{T} c_i(\tau) c_j^\dagger(0) \right\rangle . \tag{B.2}$$

The solution is

$$\mathbf{G}(i\omega_m) = (i\omega_m - \mathbf{T})^{-1} . \tag{B.3}$$

Here $\mathbf{G}$ and $\mathbf{T}$ are now matrices in the basis introduced above and the fermionic Matsubara frequencies are given by

$$i\omega_m = i\frac{\pi}{\beta}(2m+1) . \tag{B.4}$$

Let us now derive this simple and beautiful result. First, note that the operators are in the modified Heisenberg picture

$$O(\tau) = e^{\tau H} O e^{-\tau H} \tag{B.5}$$

and thus the modified Heisenberg equation of motion holds

$$-\frac{\partial}{\partial \tau} O(\tau) = [O, H]_- . \tag{B.6}$$

We compute the commutator of the annihilator and the Hamiltonian

$$[c_l, H]_- = \sum_{i,j} T_{i,j} \left[c_l, c_i^\dagger c_j \right] = \sum_{i,j} T_{i,j} \delta_{l,i} c_j = \sum_j T_{l,j} c_j \tag{B.7}$$

and take the derivative of the Green's function with respect to the imaginary time.

$$
\begin{aligned}
-\frac{\partial}{\partial \tau} G_{i,j}(\tau) &= \frac{\partial}{\partial \tau} \left\langle \mathcal{T} c_i(\tau) c_j^\dagger(0) \right\rangle \\
&= \frac{\partial}{\partial \tau} \left(\theta(\tau) \left\langle c_i(\tau) c_j^\dagger(0) \right\rangle - \theta(-\tau) \left\langle c_j^\dagger(0) c_i(\tau) \right\rangle \right) \\
&= \delta(\tau) \left(\left\langle c_i(\tau) c_j^\dagger(0) \right\rangle + \left\langle c_j^\dagger(0) c_i(\tau) \right\rangle \right) + \left\langle \mathcal{T} \frac{\partial}{\partial \tau} c_i(\tau) c_j^\dagger(0) \right\rangle \\
&= \delta(\tau) \left\langle \left[c_i(\tau), c_j^\dagger(0) \right]_+ \right\rangle - \left\langle \mathcal{T} \left[c_i(\tau), H \right]_- c_j^\dagger(0) \right\rangle \\
&= \delta(\tau) \left\langle \left[c_i(0), c_j^\dagger(0) \right]_+ \right\rangle - \sum_j T_{i,j} \left\langle \mathcal{T} c_i(\tau) c_j^\dagger(0) \right\rangle \\
&= \delta(\tau) \delta_{i,j} + \sum_j T_{i,j} G_{i,j}(\tau)
\end{aligned}
\tag{B.8}
$$

The imaginary time Green's function can be expanded in a Fourier series

$$
G_{i,j}(\tau) = \frac{1}{\beta} \sum_m G(i\omega_m) e^{-i\omega_m \tau}, \tag{B.9}
$$

where $G(i\omega_m)$ is the energy space Matsubara Green's function. Again taking the derivative with respect to τ and setting equal to (B.8) yields

$$
\frac{1}{\beta} \sum_m G_{i,j}(i\omega_m) (-i\omega_m) e^{-i\omega_m \tau} = -\delta(\tau) \delta_{i,j} - \sum_j T_{i,j} \frac{1}{\beta} \sum_m G(i\omega_m) e^{-i\omega_m \tau}. \tag{B.10}
$$

Noting that $\delta_{n,m} = \frac{1}{\beta} \int_0^\beta d\tau\, e^{i(\omega_n - \omega_m)\tau}$ we consequently multiply with $e^{i\omega_n \tau}$, integrate over τ and finally arrive at

$$
-i\omega_m G_{i,j}(i\omega_m) = -\delta_{i,j} - \sum_j T_{i,j} G_{i,j}(i\omega_m) \tag{B.11}
$$

which is easily rewritten in matrix form

$$
i\omega_m \mathbf{G}(i\omega_m) = \mathbf{1} + \mathbf{T}\,\mathbf{G}(i\omega_m), \tag{B.12}
$$

$$
\mathbf{G}(i\omega_m) = (i\omega_m - \mathbf{T})^{-1}. \tag{B.13}
$$

But that's just our result (B.3) stated in the beginning. Symbolically we can write equivalently

$$
G(i\omega_m) = \frac{1}{i\omega_m - H}, \tag{B.14}
$$

which we understand as taken with respect to a basis $|i\rangle$.

BIBLIOGRAPHY

[1] P. W. Anderson, "Localized Magnetic States in Metals," *Phys. Rev.* **124** (Oct, 1961) 41–53. (Cited on pages 1 and 21.)

[2] P. W. Anderson, "A poor man's derivation of scaling laws for the Kondo problem," *Journal of Physics C: Solid State Physics* **3** (1970) 2436–2441. `http://stacks.iop.org/0022-3719/3/2436`. (Cited on page 2.)

[3] J. E. Hirsch and R. M. Fye, "Monte Carlo Method for Magnetic Impurities in Metals," *Phys. Rev. Lett.* **56** (Jun, 1986) 2521–2524. (Cited on page 2.)

[4] J. E. Hirsch, "Discrete Hubbard-Stratonovich transformation for fermion lattice models," *Phys. Rev. B* **28** (Oct, 1983) 4059–4061. (Cited on page 2.)

[5] A. N. Rubtsov, V. V. Savkin, and A. I. Lichtenstein, "Continuous-time quantum Monte Carlo method for fermions," *Phys. Rev. B* **72** (Jul, 2005) 035122. (Cited on pages 2 and 9.)

[6] P. Werner, A. Comanac, L. de' Medici, M. Troyer, and A. J. Millis, "Continuous-Time Solver for Quantum Impurity Models," *Phys. Rev. Lett.* **97** (Aug, 2006) 076405. (Cited on page 3.)

[7] F. Goth, "A Quantum Monte-Carlo method for systems out of equilibrium," Master's thesis, Universität Würzburg, Sep, 2009. (Cited on page 3.)

[8] A. Georges, G. Kotliar, W. Krauth, and M. J. Rozenberg, "Dynamical mean-field theory of strongly correlated fermion systems and the limit of infinite dimensions," *Rev. Mod. Phys.* **68** (Jan, 1996) 13. (Cited on page 3.)

[9] D. J. Luitz and F. F. Assaad, "A weak coupling CTQMC study of the single impurity and periodic Anderson models with s-wave superconducting baths," `arXiv:0909.2656v2 [cond-mat.str-el]`. `http://arxiv.org/abs/0909.2656v2`. (Cited on page 3.)

[10] M. Potthoff, *Lecture notes: Anwendungen der Viel-Teilchen-Theorie in der Festkörperphysik.* 2008.

`http://www.physnet.uni-hamburg.de/hp/mpotthof/vvtt08/diagrams.pdf`.
(Cited on page 5.)

[11] P. Coleman, *The evolving monogram on Many Body Physics*. 2009.
`http://www.physics.rutgers.edu/~coleman/`. (Cited on page 5.)

[12] F. F. Assaad and T. C. Lang, "Diagrammatic determinantal quantum Monte
Carlo methods: Projective schemes and applications to the Hubbard-Holstein
model," *Phys. Rev. B* **76** (Jul, 2007) 035116. (Cited on pages 5, 9, 26, and 27.)

[13] F. F. Assaad, *Draft of a book on quantum Monte Carlo methods*. unpublished, 2006.
(Cited on pages 10 and 13.)

[14] P. Young, *Jackknife and Bootstrap Resampling Methods in Statistical Analysis to
Correct for Bias*. `http://apyoung.com/~peter/jackboot.pdf`. (Cited on page 20.)

[15] D. J. Luitz, "Anwendung der Diagrammatischen Monte Carlo Methode auf den
Josephson Strom durch einen Kondo-Quantenpunkt," Master's thesis,
Universität Würzburg, Aug, 2008. (Cited on page 29.)

[16] A. C. Hewson, *The Kondo Problem to Heavy Fermions*. Cambridge Studies in
Magnetism. Cambridge University Press, 1993. (Cited on pages 32, 33, 34,
and 37.)

[17] F. Mancini, ed., *Lectures on the physics of highly correlated electron systems VI*,
vol. 629 of *AIP Conference Proceedings*. American Institue of Physics, 2002. (Cited
on page 32.)

[18] M. Potthoff, *Lecture notes: Vielteilchentheorie*. 2008.
`http://www.physnet.uni-hamburg.de/hp/mpotthof/vvtt08/manuskript.pdf`.
(Cited on page 32.)

DECLARATION

Ich versichere hiermit, dass ich die vorgelegte Diplomarbeit am Institut für Theoretische Physik und Astrophysik der Julius-Maximilians-Universität Würzburg unter der Anleitung von Prof. Dr. Fakher F. Assaad selbstständig durchgeführt und keine anderen Quellen und Hilfsmittel als die angegebenen benutzt habe.

Würzburg, December 2009

Burkhard Ritter